5/172013

Wheel Induced Vibrations on Heavy Vehicles

Emma Smith and Hector Garcia

SA105X DEGREE PROJECT IN VEHICLE ENGINEERING, FIRST LEVEL

Abstract

Some of the most significant comfort disturbances in heavy vehicles can often be related to the wheels. In those cases, the vibration of the vehicle is excited by for example force variations within the tire, ovality of the tire or imbalance in the wheel. The disturbances are dependent on vehicle speed and are often perceived as most unpleasant at cruising speed on a motorway, at around 90 km/h.

Truck manufacturers want to increase the robustness against this type of disturbance, since this results in an improved operator comfort. But it also makes it possible to lower the requirements on the suppliers of tires and rims, and thereby there is a financial gain for both customer and manufacturer.

The aim with this project is to increase the understanding of wheel induced vibrations. In order to achieve this a literature survey has been performed on the subject. Furthermore, the phenomenon has been studied analytically by using a quarter car model which includes a brush tire model. The model is scripted in MATLAB.

Simulations have been performed to analyse the effect on the chassis when forces excited by mass imbalance and radial run out are introduced.

When looking at the second harmonic radial run out imperfection the unsprung mass, i.e the wheel, starts to bounce during the settling time.

Also when comparing two different weights of a mass imbalance the power increase of the vibration in the sprung mass is much larger than the power increase of the unsprung mass at the specific frequency. This implies that the excitation frequency, the wheel rotation frequency in this case, is a harmonic repetition of the sprung mass undamped natural frequency.

To avoid this phenomenon the undamped natural frequency of the sprung mass must change either by adding a damper or by changing the weight or the spring stiffness. The simulation is run with a damper although without it the power increase would be much larger.

Table of contents

1. Introduction

The most significant discomfort felt by truck drivers is connected to vibrations caused by wheel and tire imperfections. Examples of these kind of imperfections are wheel imbalance, force variations and ovality of the tire. Since manufactures spend a lot of money on perfecting their vehicles for maximal comfort, finding better solutions for vibration isolation is essential. Solutions that are less complicated and time consuming will cheapen the process, improve comfort and lessen demands on suppliers.

The aim of this report is to analyse and understand the emergence of vibrations induced by wheels and tires on trucks. In order to do this, a literature survey has been performed on the subject. To understand the phenomenon further, an analysis has been made of a truck model. The model consists of a quarter car model combined with a physical tire model, together representing the front axle dynamics of a truck. Figure 1 shows the front axle of a truck of the same dimensions as the one used in the model. Frequency and power spectral analysis are used to investigate the models behaviour during different load cases, connected to wheel/tire non-uniformities.

When it comes to the model, a few assumptions and simplifications have been made. The road surface is assumed to be smooth, since the wheel forces caused by non-uniformities are usually only significant for relatively smooth roads, where they can be of the same magnitude as the forces generated by road excitation [1]. In the tire model, the amount of tread slices (the bristles of rubber on the tire surface) are kept constant. The tire model can interpret vibrations and force variations in all directions, but the study has been limited to simulations in the vertical direction. This tire damping is assumed to be zero.

Our supervisor is Assistant Professor Jenny Jerrelind, and she has guided us through-out the whole process. The model was supplied and written by PhD-student Johannes Edrén, who has helped us with some add-ons and an explanatory introduction to the model itself.

The outline of the report is as follows. Chapter 2 introduces tire and wheel imperfections, what causes them and the effects of their presence. Thereafter, in Chapter 3, the model and method are described. In Chapter 4, the results are presented and discussed. Thereafter Chapter 5 features a reflection and an analysis of the results. These chapters are followed by references, and appendixes including the MATLAB-script of the model and all load cases.

Figure 1 – Scania r620 [1].

2. Tire/Wheel non-uniformities

There are three directions of forces that are of interest when analysing tire vibrations. Lateral, tractive and radial forces. Lateral forces are perpendicular to the direction of motion and cause wobble, tractive forces are forces in the direction of travel, and radial forces are forces out from the centre of the wheel, i.e. centrifugal forces. The causes of the variation of these forces are divided into three groups; mass imbalance, geometry variations and stiffness.

2.1 Mass Imbalance

An unbalanced system is an asymmetric system, and an asymmetric system is a system which isn't optimally behaved. There are two different kinds of mass imbalance in the front wheel-tire-assembly, dynamic and static imbalance.

A non-uniform and asymmetric mass along the axis of rotation is the cause of *dynamic imbalance*. This imperfection results in torque variations perpendicular to the rotational axis.

Static imbalance is when there is asymmetry of mass along or about the axis of rotation. This kind of imbalance causes deviations of radial (centrifugal) and tangential forces.

Both dynamic and static imbalance are functions of speed, and therefore higher speeds cause more vibrations. These two types of imperfections can exist together, but one can also exist while the other one doesn't [2-3]. See Figure 2 for a closer understanding of forces acting during imbalance.

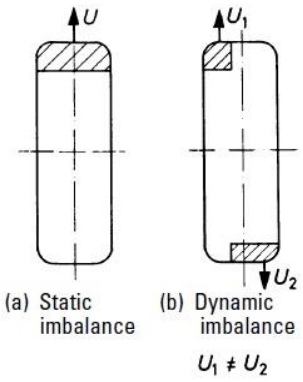

Figure 2 – Mass imbalance on wheels in rotation [8].

2.2 Geometry variations

Variations in the geometry of a tire, usually due to manufacturing errors, have disruptive effects on the ride of a vehicle. Some of the effects are listed below;

- *Radial run-out* affects the roundness of the wheel. Radial irregularity causes the tire to adopt an asymmetric shape; eccentric, oval, triangular or square, and therefore the wheel rolls irregularly [2]. Figure 3 shows the first four harmonics of radial run-out.

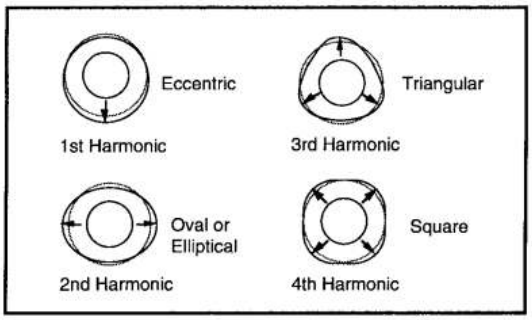

Figure 3 – Radial run-out, first four harmonics [8].

- *Lateral run-out* is the deviation of the sidewalls, of the tire, from a perfect plane. This causes vibrations, like all other imperfections, but the contribution towards the overall ride is very small compared to radial run-out [3].

- *Belt run-out* is when the belt ring is off centre from the centre of rotation. This kind of run-out is included in mass imbalance as well, seeing as the belt's mass isn't centred. The effect of belt run-out is the variation of tractive forces, causing a radius deviation of the wheel assembly [4].

- *Tread gauge variation* indicates a difference in the thickness and/or length of the tires tread slices [4].

2.3 Tire Stiffness

The elasticity of a tire can be compared to that of springs, all pointing out from the centre of the wheel. The variation in stiffness of the elastic parts of the tire can be described with the theory of springs – the springs can have different lengths in their compressed state, which causes inconsistent stiffness. This analogy gives quite a good idea of how stiffness can be interpreted when discussing tires.

Tires have a body of rubberised fabric underneath the tread for stability. The difference between bias tires and radial tires is the direction of the chords in the fore mentioned fabric body. Bias tires have two or more plies with cords in a 35 to 40 degrees angle to the circumference ([6], p. 69). Radial tires have parallel plies that are places in a 90 degree angle to the circumference. They also have a belt between the body and the tread, made up of fabric or steel wire, whose cords are roughly in a 20 degree angle to the tread. This belt helps keeping the tread flat on the road during cornering.

Nowadays, as is the case for most vehicles, trucks have radial tires as steer tires. Variations of stiffness in radial tires are due to manufacturing errors, and since these are most certainly uncommon, only one tire will be affected. And even if two tires are affected, they will most certainly be a phase shift between the tires, and so the ride will be uneven – causing vibrations [2]. Figure 4 shows how the wheel rolls unevenly due to stiffness variation.

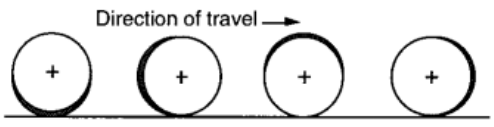

Figure 4 – Uneven roll due to stiffness variations [8].

3. Model, Method and Parameters

This chapter introduces the MATLAB-model, how it has been used and what parameters the simulations are based on.

3.1 Quarter car model

The tire non-uniformities excite movement in the truck through the spring and shock absorber. To simulate this, a quarter car model has been used together with a physical tire model. The quarter car model consists of two masses, two springs and two dampers, as seen in Figure 5. In this model, the tire's spring and damper are embedded in the physical tire model. The index ´s´ being for sprung mass, ´u´ for un-sprung mass, and ´t´ for tire.

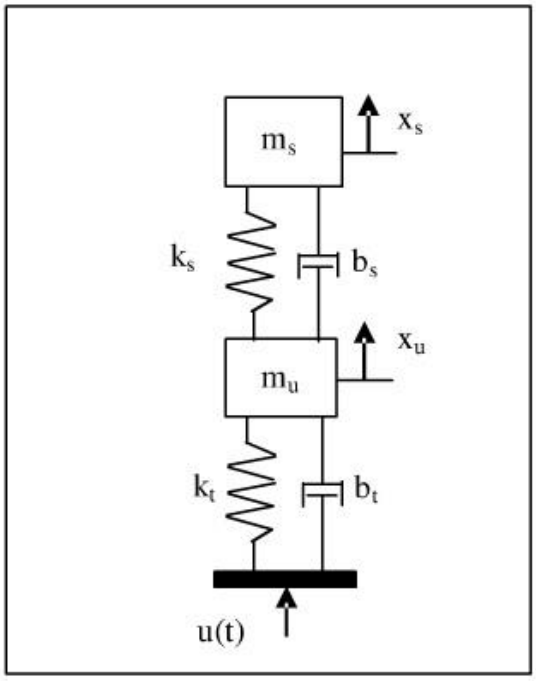

Figure 5 – Quarter car model's basic set-up.

This two DOF system has two equations of motion;

$$m_s\ddot{x}_s + b_s(\dot{x}_s - \dot{x}_u) + k_s(x_s - x_u) = -m_s g \quad (1)$$

$$m_u\ddot{x}_u - b_s(\dot{x}_s - \dot{x}_u) - k_s(x_s - x_u) + b_t\dot{x}_u + k_t x_u = k_t h + b_t h - \dot{m}_u g \quad (2)$$

Dividing both equations with the corresponding masses, the acceleration of each body can be calculated, which can be derived from Newton's second law;

$$\ddot{x}_s = \frac{b_s(\dot{x}_u - \dot{x}_s) + k_s(x_u - x_s)}{m_s} - g \tag{3}$$

$$\ddot{x}_u = \frac{k_t h + b_t \dot{h} + b_s(\dot{x}_s - \dot{x}_u) + k_s(x_s - x_u) - b_t \dot{x}_u - k_t x_u}{m_u} - g \tag{4}$$

These accelerations are then transferred from time domain to frequency domain using Fourier transform. This makes it possible to produce a graph showing at which frequencies the vibrations cause the greatest accelerations within the different components.

To simulate the mass imbalance in the tire and rim, a centrifugal force is added to the wheel centre. This force can then be phase shifted to move it around the circumference of the tire in the starting position. The phase shift is only varied when several non-uniformities are combined in one simulation so that the faults don't end up at the same place in the wheel. The equation used to implement mass imbalance in the model is as follows;

$$F_{imb} = m_{imb} \cdot r_{imb} \cdot \omega^2 \cdot \sin(\theta + \varphi) \tag{5}$$

m_{imb} is the mass of the imbalance, r_{imb} is the radius on which the mass is positioned, ω is the angular speed of the wheel, θ is the position of the mass, and φ is the phase shift. This force is then added to Equation (4) as follows;

$$\ddot{x}_u = \frac{k_t h + b_t \dot{h} + b_s(\dot{x}_s - \dot{x}_u) + k_s(x_s - x_u) - b_t \dot{x}_u - k_t x_u + F_{imb}}{m_u} - g \tag{6}$$

For this specific problem, the undamped natural frequencies are of interest to visualise approximately where in the frequency spectrum resonance will occur. To calculate these frequencies the following formulas has been used.

$$f_{unsprung} = \frac{\sqrt{k_t + k_s}}{m_u} \cdot \frac{1}{2\pi} \tag{7}$$

$$f_{sprung} = \frac{\sqrt{k_s}}{m_s} \cdot \frac{1}{2\pi} \tag{8}$$

3.2 Physical tire model

To simulate the tire physically, this part of the model is constructed using the idea of a brush with a user specified amount of bristles. The model is based on the brush tire model presented in Hans Pacejka's book ´Tire and Vehicle Dynamics` [7]. The brush is spread around a part of the circumference of the tire. As the tire rotates the brush moves along the circumference -

this is to save computer power and to shorten the time it takes to complete the simulation, since the amount of bristles can be kept down without affecting the resolution of the results.

The bristles are the only things that comes in contact with the road, hence the bristle data decides the deformation of the tire. To get good results from the tire model, the bristles are adjustable in both damping and spring stiffness in all directions. In this study however, the vertical direction is the only direction evaluated.

To simulate radial run-out, the circumference of the tire is varied by adding a sinus curve, which in turn can be adjusted to obtain different harmonic repetitions of the run-out.

The road surface is also adjustable to simulate road roughness, although for this project the road surface is set as perfectly smooth. This is to keep focus on the tire imperfections, and not confuse them with other discrepancies.

3.3 Flow chart of the MATLAB-model

The MATLAB-program consists of the tire model and a quarter car model. A flow chart has been made to illustrate the process of the simulation, see Figure 6. For a complete study of the MATLAB-program see Appendix B, together with all the function files.

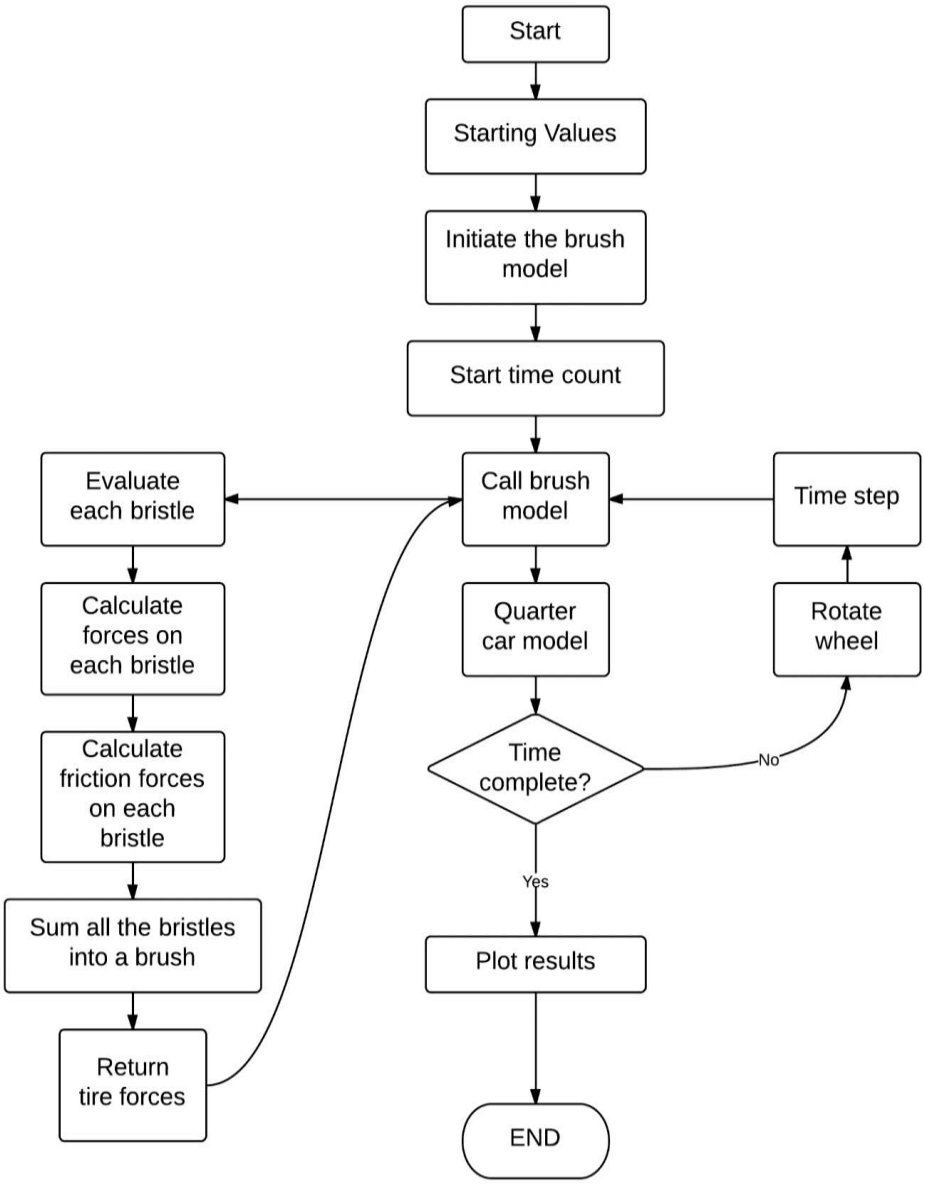

Figure 6 – Flow chart illustrating the structure of the MATLAB-script and its different parts.

3.4 Method

To make an accurate evaluation of how the imperfections affect the chassis, the MATLAB-model is simulated for different load cases. These load case have been chosen in order to represent the disturbances caused by mass imbalance and radial run-out.

The first kind of tire imperfection alternated in the model is mass imbalance. Load case 2, 7 and 8 are affected by this. In load case 2, the wheel is affected only by mass imbalance, whereas in load case 7 the mass imbalance is combined with a 90 degree phase shift and a radial run-out of the first harmonic. In load cases 3 through 6 the wheel is subjected to radial run-out of the first four harmonics. Load case 8 is a combination of two cases, each with a different mass imbalance, 0.5 kg and 8 kg. Table 1 has all the information about the load cases. The radius 0.5 m used in the load cases with mass imbalance is the radius of the wheel, and so the mass imbalance is situated on the circumference.

Table 1 – Load cases tested in MATLAB-model

LOAD CASES	**MASS IMBALANCE**			**RADIAL RUN-OUT**	
	Mass [kg]	**Radius [m]**	**Phase shift [degree]**	**Harmonic nr**	**Difference [m]**
1	0	0	0	0	0
2	2	0.5	0	0	0
3	0	0	0	1	0.005
4	0	0	0	2	0.005
5	0	0	0	3	0.005
6	0	0	0	4	0.005
7	2	0.5	90	1	0.005
8	0.5 and 8	0.5	0	0	0

Stiffness is not varied in any of the load cases. This is because stiffness variations only affect the results homogenously and the difference, if noticeable, will only be in amplitude of the force or power peaks.

According to Thomas D. Gillespie [2], higher order harmonics of radial run-out are unnecessary to include in a survey about ride perception, as they show similar information only in smaller magnitude at higher frequencies. Also, the magnitude of radial force variations is relatively independent of speed, only the frequency is changed. It is therefore sufficient to investigate the first four harmonics of radial run-out.

In Deodhar, Rakheja and Bhat's report about vibration and tire force transmissibility, it is mentioned that radial run-out is a much larger cause of vibrations than tangential and lateral geometry variations [5].

Both reports state that radial run-out is an important, if not vital, part of vibration analysis. This has been taken into consideration when the load cases were chosen, hence the large percentage of load cases where radial run-out is included.

Furthermore, in Deodhar, Rakheja and Bhat's report [5], a half car model is used to simulate load cases similar to the ones in this report. Their range of imbalance mass, for the front tire-wheel assembly, is set to 0.5 kg – 2 kg. For all load cases in this report incorporating mass imbalance, except load case 8, a mass of 2 kg has been chosen. The reason for choosing the top end of the range given by Deodhar et al. is the conviction that a larger weight will cause larger fluctuations in vibration amplitudes. The conviction is also that this will produce graphs with clearer peaks and dips.

In load case 8, the two masses have been chosen to 0.5 kg and 8 kg. This is because 0.5 kg seemed to be the lowest value still causing noticeable vibrations, and 8 kg was chosen to be unreasonably high, so as to see a striking difference in the results.

3.5 Parameters

In Table 2 the parameters for the model are specified. The vehicle model represents the front axle dynamics of a truck. The speed of the truck has been chosen to 89 km/h which is the average cruising speed of a Swedish motorway.

Table 2 – Parameters used in MATLAB-model.

Parameter	Value
Vehicle speed	89 km/h
Sprung mass	3 400 kg
Un-sprung mass	350 kg
Suspension spring stiffness	300 000 N/m
Suspension damper stiffness, compression	2 000 Ns/m
Suspension damper stiffness, expansion	20 000 Ns/m
Tire spring stiffness, vertical	800 000 N/m
Tire damper stiffness, vertical	0 Ns/m
Range of imbalance mass	0.5 – 8 kg
Radial run-out	5 mm
Phase angle	90°

4. Results and Conclusions

This chapter discusses and evaluates the results of the tests simulated with the model. Due to limitations in report length, some load cases' graphs are exclusively situated in Appendix A. Load case 1, 2, 4 and 8 show the most distinct results, and are therefore discussed more closely.

Table 3 shows the calculated natural undamped frequencies and the wheel rotation frequency.

Table 3 – Resonance frequencies.

Frequency	Value [Hz]
Wheel rotation frequency	7.5406
Undamped natural frequency, sprung mass	1.4950
Undamped natural frequency, unsprung mass	24.5090

4.1 Load case 1

This load case reveals what forces and vibrations would be on a tire without any exterior forces or geometry variations. The tire is perfectly round and symmetrical, and the centre of the wheel is concentric with the axis of rotation. This load case is meant as a reference case to compare the other load cases to.

In Figure 7, the settling forces that occur when the system is released from the starting position are visualised by fluctuations at low frequencies. These fluctuations will be present in all following graphs, in somewhat different shapes and forms.

Since the tire and road are without imperfections, the forces of the sprung mass (chassis) and unsprung mass (tire) will be similar to each other. The amplitudes, shown by the green and blue lines, will therefore be co-linear.

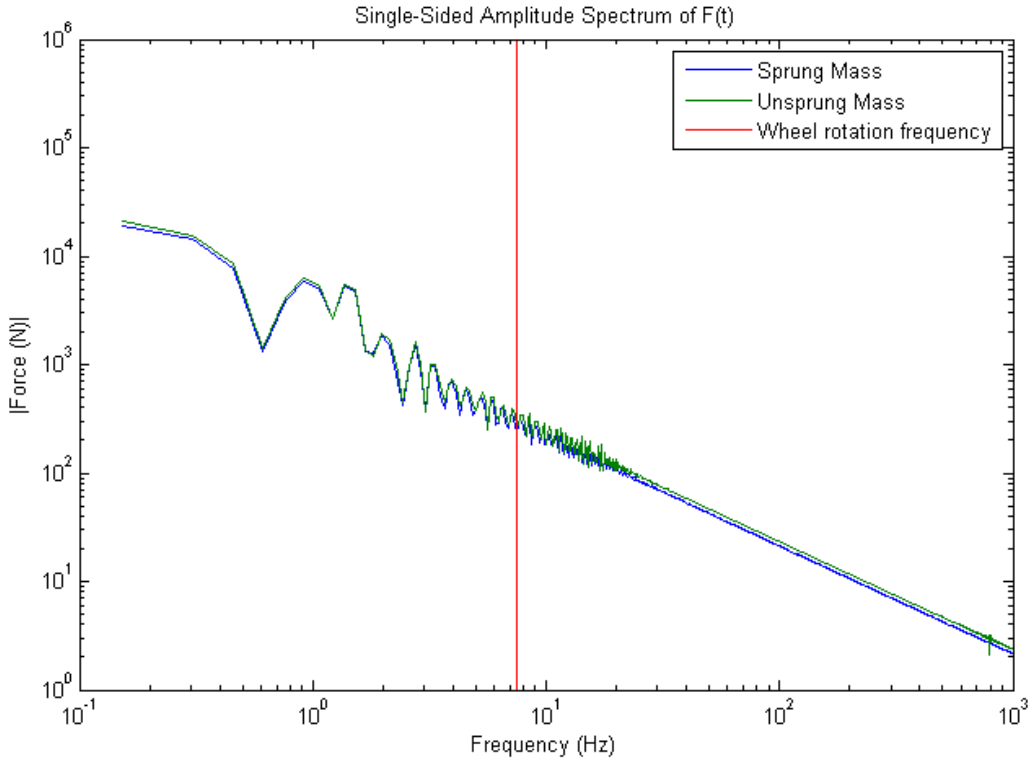

Figure 7 – Vertical force amplitude as a function of frequency.

The power spectral density graph below, Figure 8, shows where in the frequency spectra the vibrations have the largest energy per second. This does not mean that the vibration amplitudes have to be very big, just that the transmitted effect is large and more difficult to cancel out.

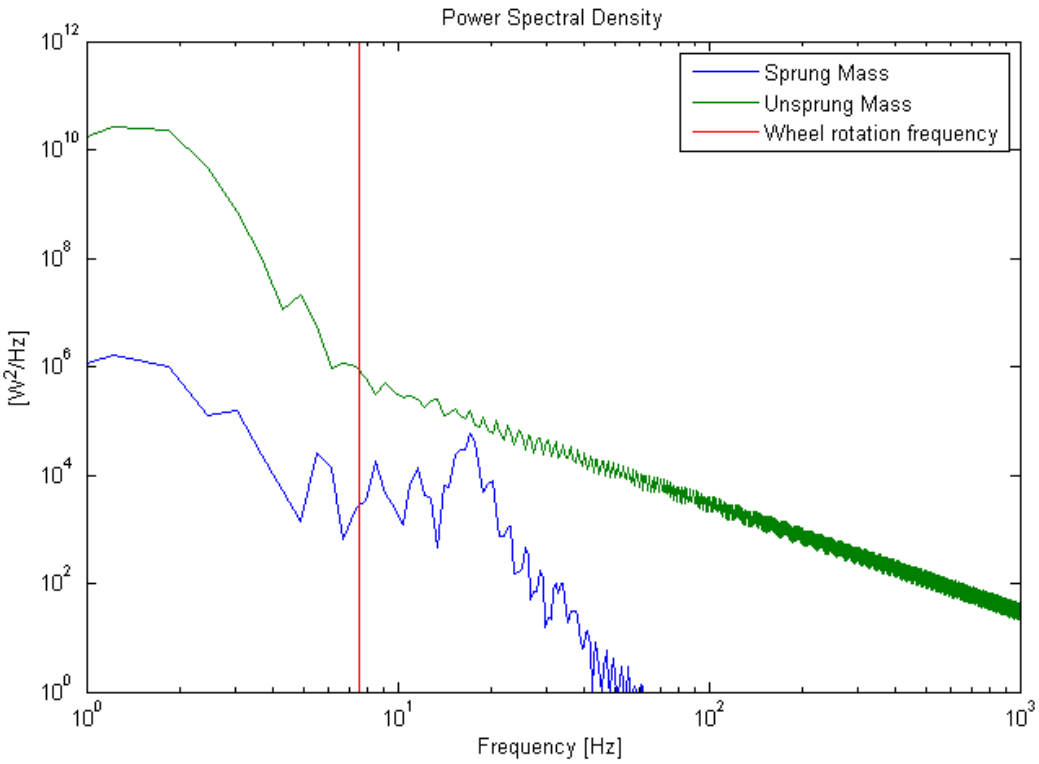

Figure 8 – Power spectral density graph.

4.2 Load case 2

In this load case, the tire is laden with a mass imbalance of 2 kg, situated on the circumference.

As expected, Figure 9 shows a peak in the force of both the sprung and unsprung masses at the wheel rotation frequency. This is due to having a single mass imbalance adding a centrifugal force to the wheel centre, and since the mass imbalance rotates at the same velocity as the wheel, their frequencies will coincide.

The force amplitude is almost ten times higher for the unsprung mass than for the sprung mass. This is because the spring and damper in the strut absorb a lot of the forces caused by the mass imbalance in the tire.

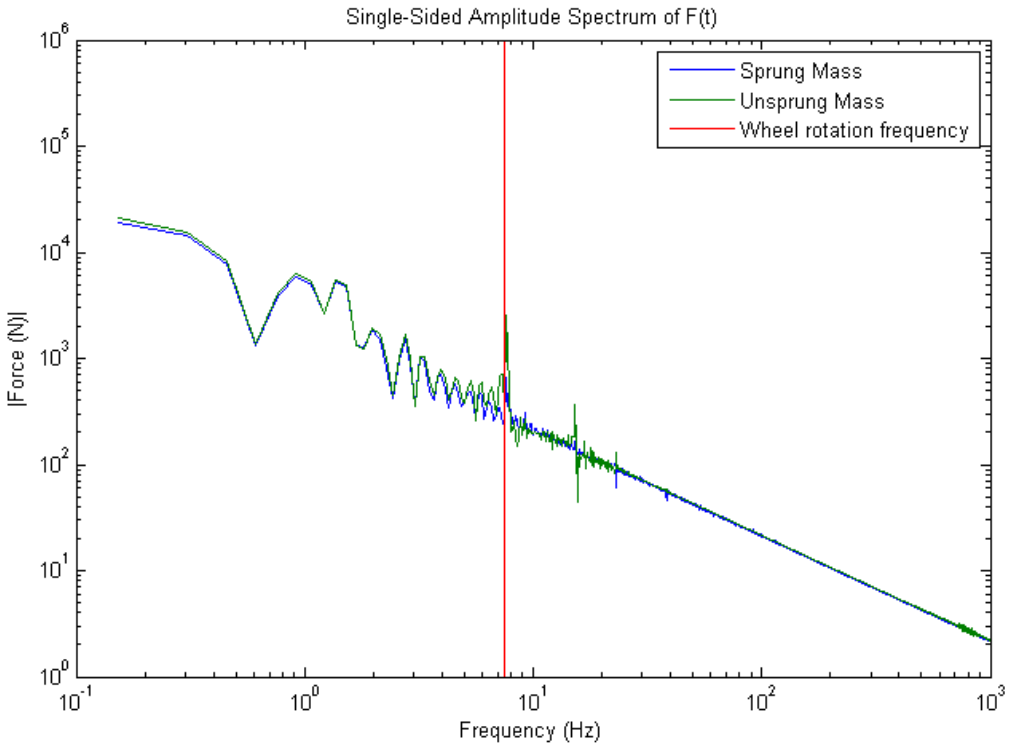

Figure 9 – Vertical force amplitude as a function of frequency.

Figure 10 shows that the relationship between tire and chassis is reversed when comparing power instead of force, at the wheel rotation frequency. The increase of power in the sprung mass is much greater, which implies that the wheel rotation frequency must coincide with a resonance frequency.

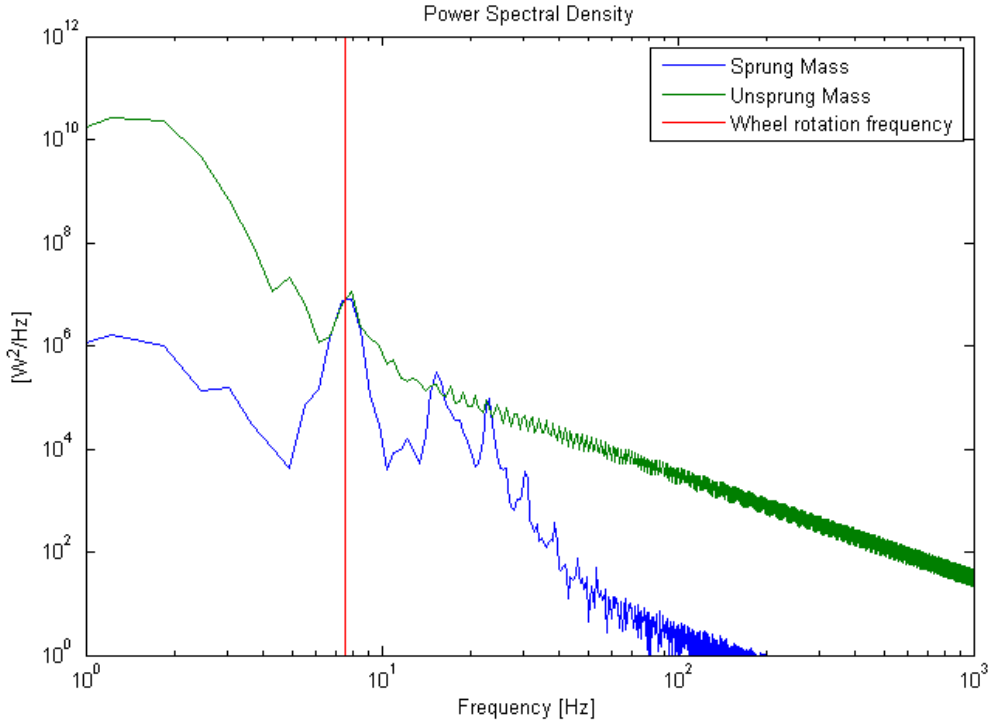

Figure 10 – Power spectral density graph.

4.3 Load case 4

Load case 4 presents a tire with a radial run-out of the 2nd harmonic. The difference in radius is 5 mm in two places opposite to each other, making the tire oval.

Figure 11 shows that the first force amplitude peak occurs at around 14-15 Hz, which is very close to the second harmonic of the wheel rotation frequency. This was expected due to the fact that there are two "bumps" on opposite sides of the circumference. Compared to load case 2, there are now two excitation forces per revolution, thus the doubled frequency.

The following peaks are the harmonic repetitions of the excited vibration. After these clear peaks, the simulation result seems to have a lot of noise, although this is not the case. It only appears so due to the logarithmic scale.

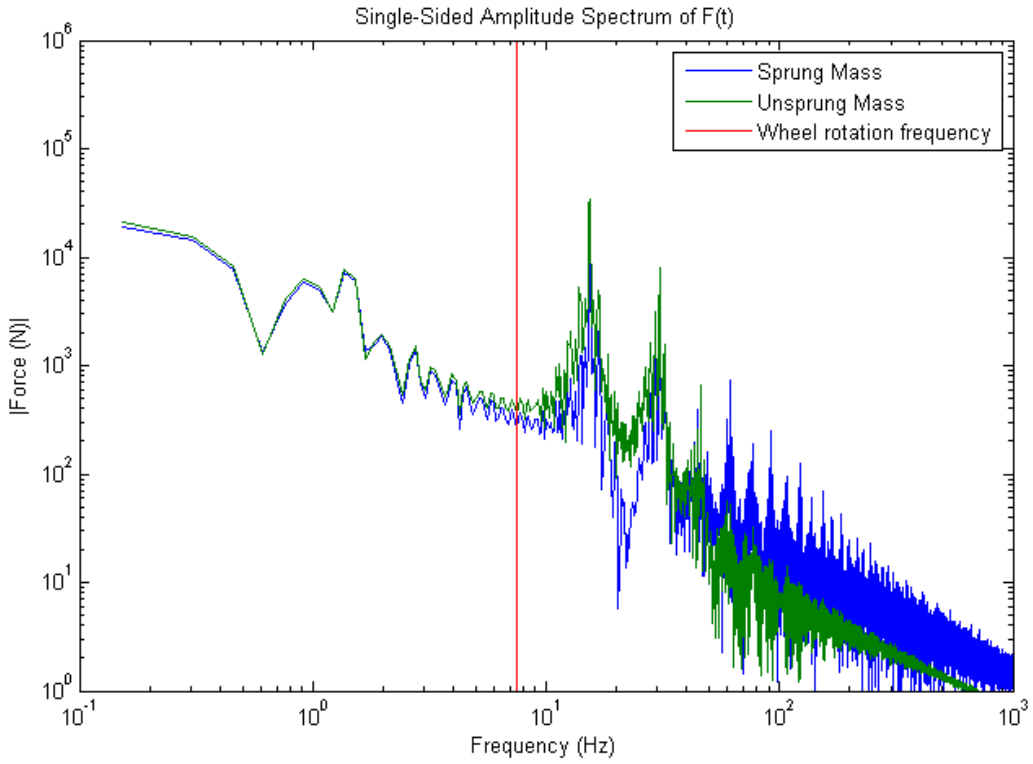

Figure 11 – Vertical force amplitude as a function of frequency.

The power spectral density of load case 4, visualised in figure 12, shows how a large power increase in the higher frequency spectra. The wheel, during this simulation, leaves the ground when bouncing immediately after being let go from the starting position. Therefore it is possible to see a large dip in the force-frequency graph, Figure 11, and a smaller first peak in Figure 12. The force at this point will decrease immensely in size, and the largest peak in the power spectral density graph will therefore come after this point, when the wheel regains contact with the road. The highest peak in Figure 12 is at a frequency of 30 Hz, and is the second harmonic of the vibration frequency. In Figure 12 we can also see that the power affecting the sprung mass grows larger than the power affecting the unsprung mass, which indicates that a radial run-out of the 2nd harmonic excites vibrations with a lot of power to the sprung mass, i.e. the chassis.

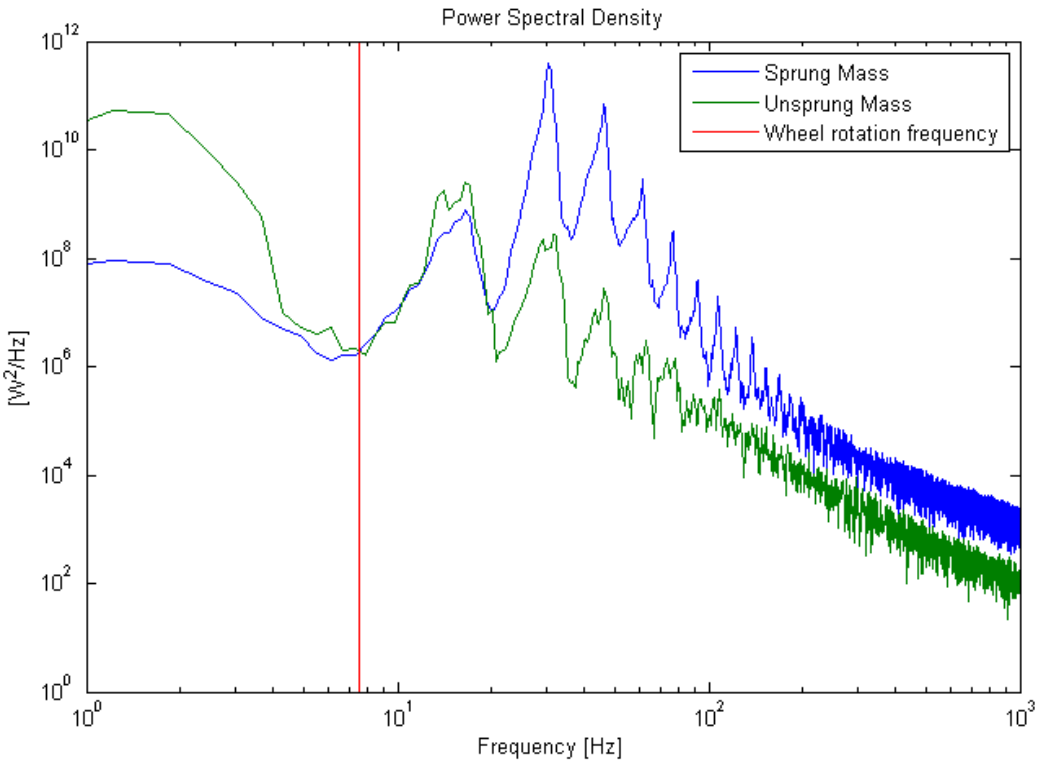

Figure 12 – Power spectral density graph.

4.4 Load case 8

This load case is made up of two different load cases, compared in the same graphs. They both consist of a tire with a mass imbalance; one of 8 kg and the other of 0.5 kg, both on the circumference.

Figure 13 shows the amplitude spectrum of the forces affecting the chassis through the strut. The lower frequencies forces come from the settling of the truck after releasing it from the starting position. These forces will not be considered in the analysis. The peak close to the wheel rotational frequency is the force that repeatedly excites the chassis, causing vibration to the driver. The weight increase of the mass imbalance in the tire assembly does not affect where in the frequency spectra the forces act, although it does change the amount of force acting on the strut.

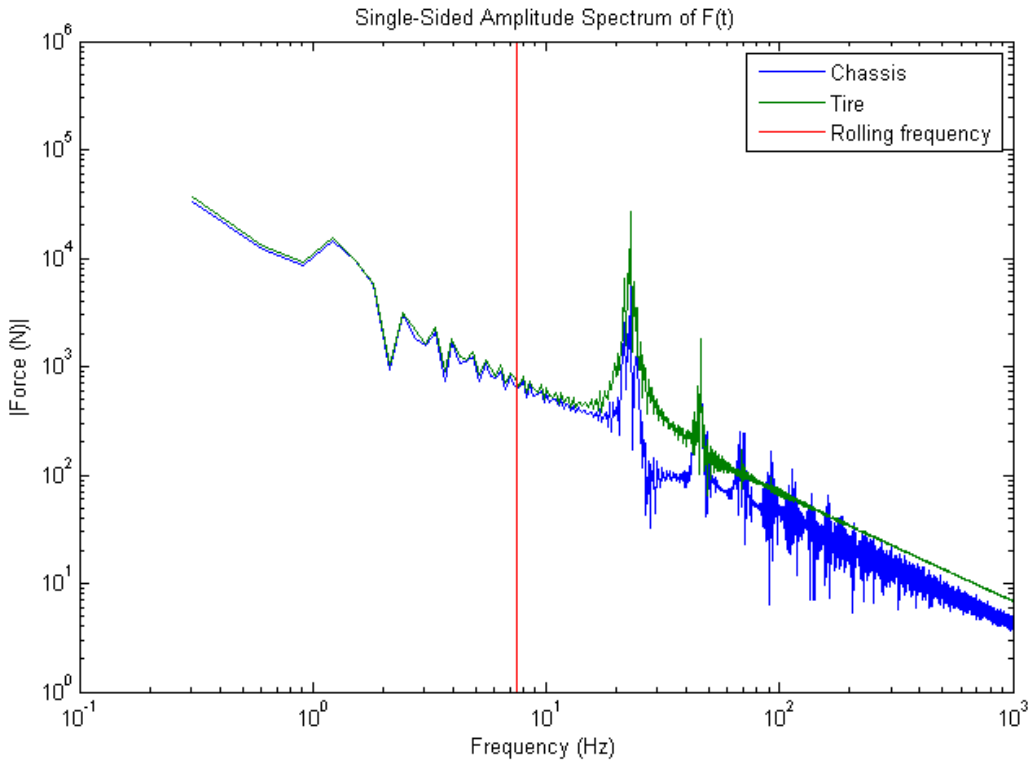

Figure 13 – Force amplitude over frequency spectra.

By drastically changing the weight of the mass imbalance it is possible to visualize how the variation of mass of the imballance affect the chassis and the tire. Studying the the purple line in Figure 14, which represents the wheel rotational frequency of the tire which is 7.54 Hz at the rolling speed of 89 km/h, it is clear that there is a power increase for both the tire and chassis. Also visible in the figure are the undamped natural frequencies these were added for comparison with the power peaks.

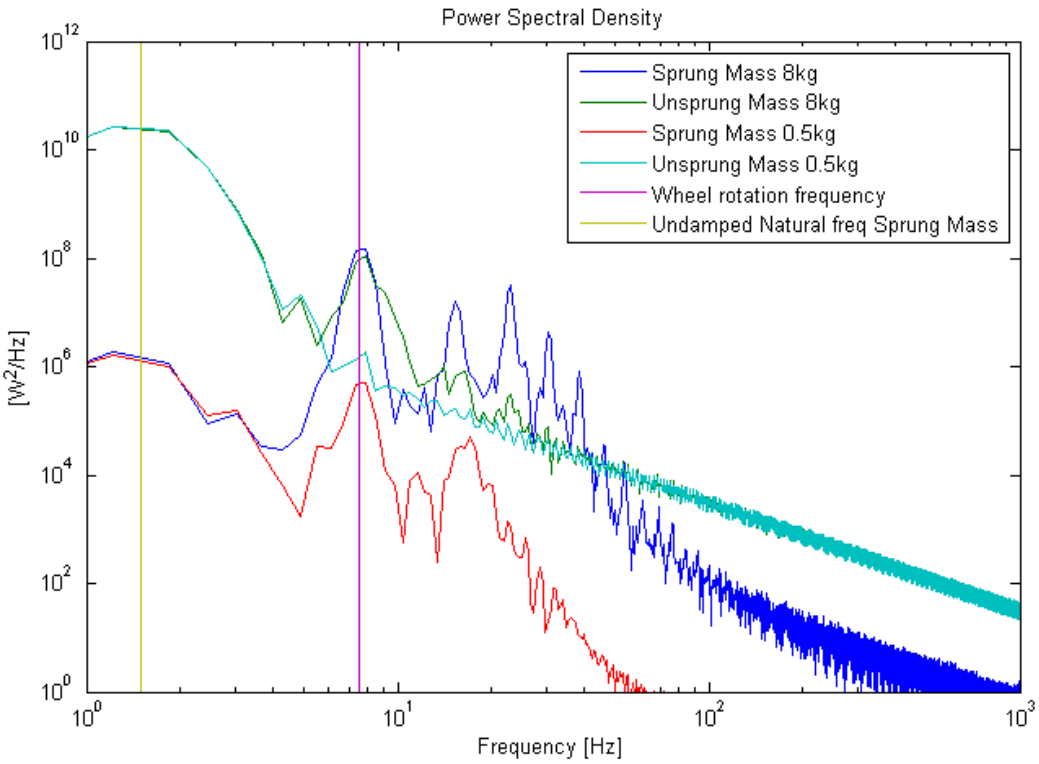

Figure 14 – Power spectral density graph.

5. Reflection, Discussion and Analysis

When looking at the PSD graphs, comparing the undamped natural frequencies of the chassis to the wheel rotation frequency of the tire, it becomes clear that the power peaks coincide with these frequencies. It can also be seen that the power increase of the chassis' vibrations is larger than the power increase of the tire's vibrations. This suggests that a harmonic repetition of the natural frequency of the chassis is very close to the rolling frequency. When dividing the rolling frequency with the undamped natural frequency of the chassis, results show that the rolling frequency is almost equal to the 5th harmonic repetition of the chassis natural frequency.

These results imply that vibrations excited to the chassis (from the wheels, through the strut) will multiply in amplitude due to the fact that the natural frequency coincides with a harmonic of the rolling frequency. The consequences are unnecessarily large vibrations, and there are ways to solve this. To overcome this problem the natural frequency of the chassis must be changed, either by changing the weight of the vehicle or the spring stiffness.

Load case four should be a subject for future analysis since it is the load case which transfer most power to the sprung mass over a wide frequency spectrum.

For further analysis of the model it should be expanded with to a half car model together with the cab and driver seat. This would show what type of imperfection will have the most effect on the driver.

6. References

1. *Handbook of Vehicle-Road Interaction*
   David Cebon
   Swets & Zeitlinger B.V., 1999
   Chapter 7.4.10, page 121

2. *www.scania.se/lastiblar/lastbilsprogram/*
   Scania-Bilar Sverige AB
   2013-05-03

3. *Fundamentals of Vehicle Dynamics*
   Thomas D. Gillespie
   Society of Automotive Engineers Inc., 1992
   Chapter 5; Ride, Chapter 10; Tires.

4. *A study on the effect of different tyre imperfections on steering wheel vibration*
   N. Balaramakrishna, R. Krishna Kumar
   Vehicle System Dynamics: International Journal of Vehicle Mechanics and Mobility, 2009

5. *Tyre non-uniformities: comparison of analytical and numerical tyre models and correlation to experimentally measured data*
   Hans R. Dorfi
   Vehicle System Dynamics: International Journal of Vehicle Mechanics and Mobility, 2011

6. *Vibration and tyre force transmissibility of commercial vehicles owing to wheel unbalance and non-uniformity defects*
   Deodhar, Rakheja, Bhat
   Vehicle System Dynamics: International Journal of Vehicle Mechanics and Mobility, 2011

7. *Tires, Suspension and Handling*
   John C. Dixon
   Society of Automotive Engineers Inc., 1996
   From page 44, Second Edition

8. *Tire and Vehicle Dynamics*
   Hans Pacejka
   Elsevier Ltd., 2012
   Chapter 3

7. Appendix A – Load cases

Here in Appendix A, all the results of the load case simulations are presented. There are five different plots presented for every load case;

- A graph showing forces in the vertical direction for tire and strut, over time
- A graph showing position in the vertical direction for sprung and unsprung mass, over time
- A single-sided amplitude spectrum graph showing the for mentioned forces as a function of frequency
- A power spectral density graph showing power as a function of frequency
- A graph showing forces on the bristles as a function of their position on the tire.

7.1 Load case 1

This load case reveals what forces and vibrations would be on a tire without any exterior forces or geometry variations. The tire is perfectly round and symmetrical, and the centre of the wheel is concentric with the axis of rotation. This load case is meant as a reference case to compare the other load cases to, and the results of this load case are shown in Figures 15-18.

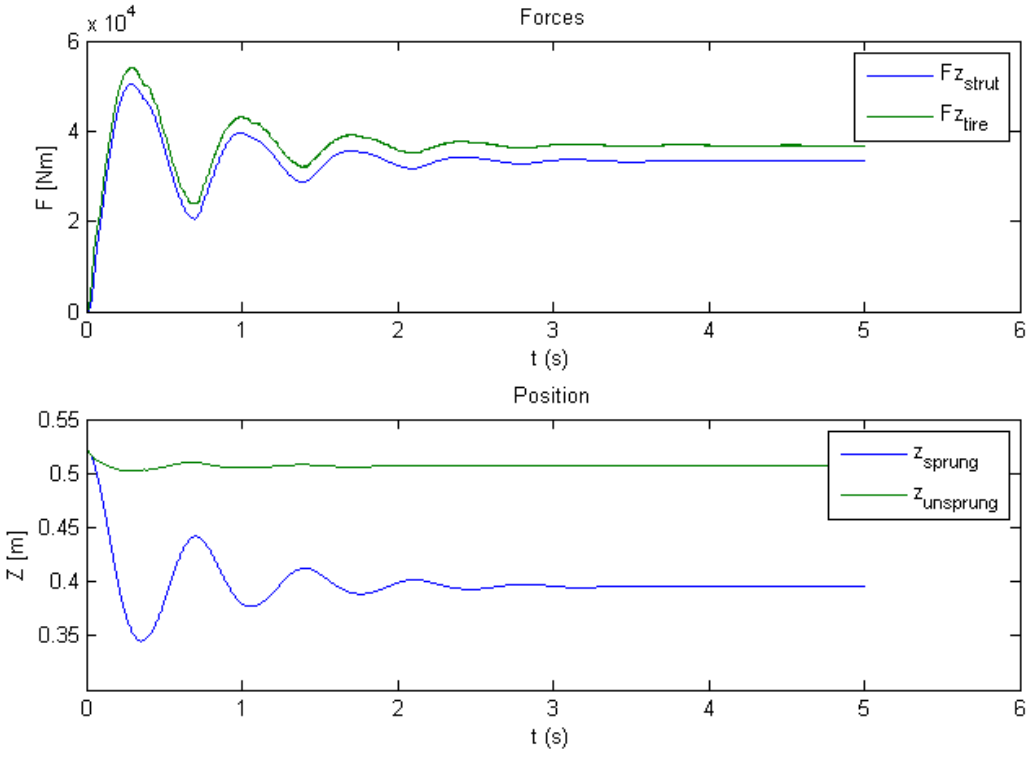

Figure 15 – Vertical forces and positions of sprung and unsprung masses, as a function of time.

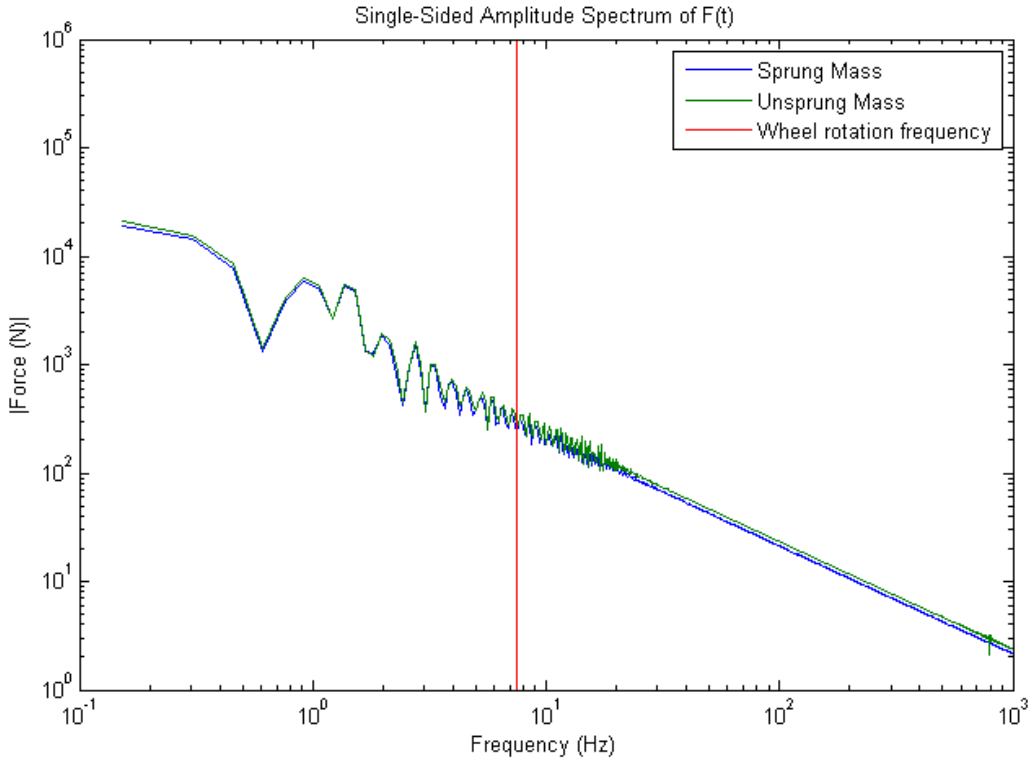

Figure 16 – Vertical force amplitude as a function of frequency.

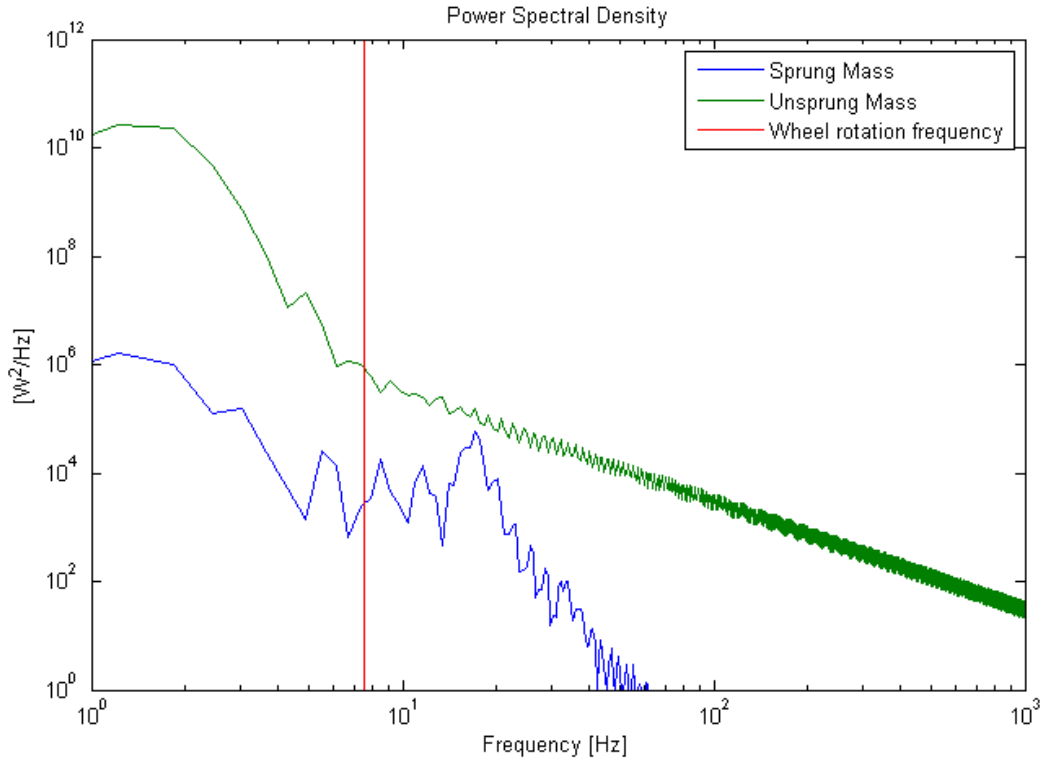

Figure 17 – Power spectral density graph.

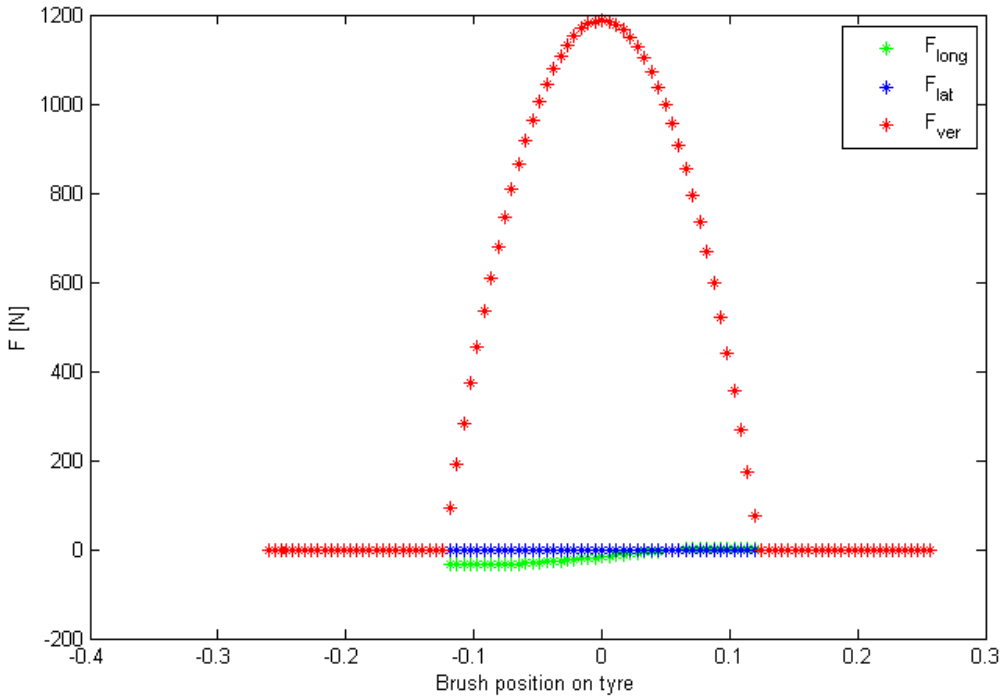

Figure 18 – Bristles forces as a function of their position on the tire.

7.2 Load case 2

In this load case, the tire is affected by a mass imbalance. The imbalance is 2 kg, on circumference. The results are shown in Figures 19-22.

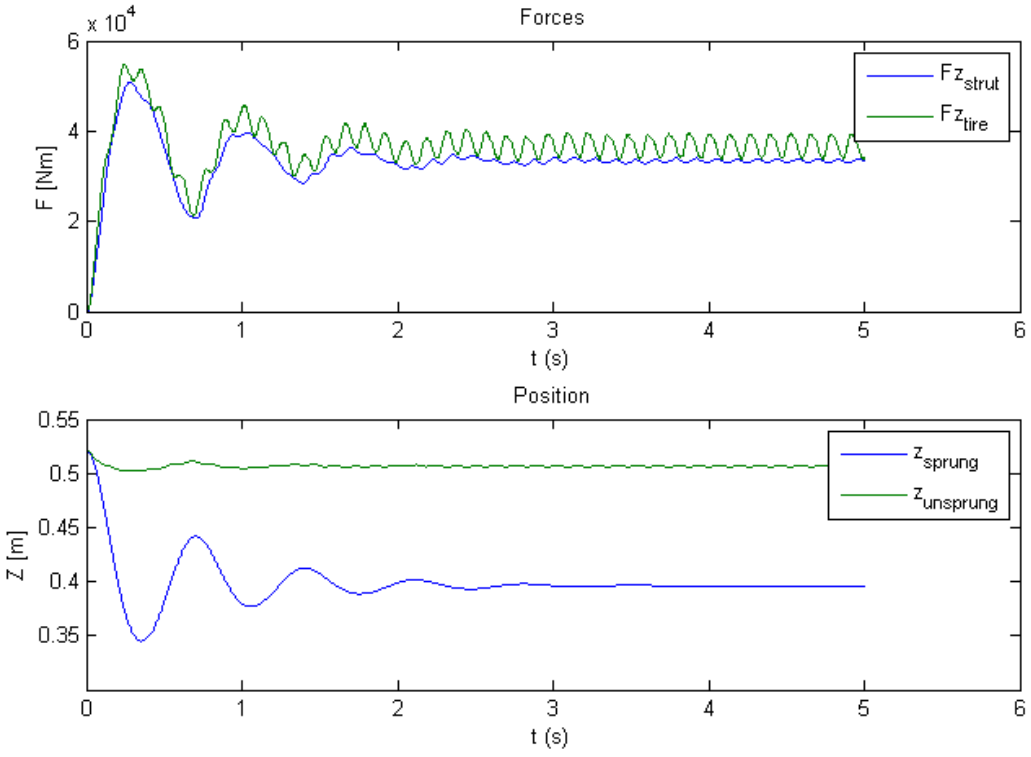

Figure 19 – Vertical forces and positions of sprung and unsprung masses, as a function of time.

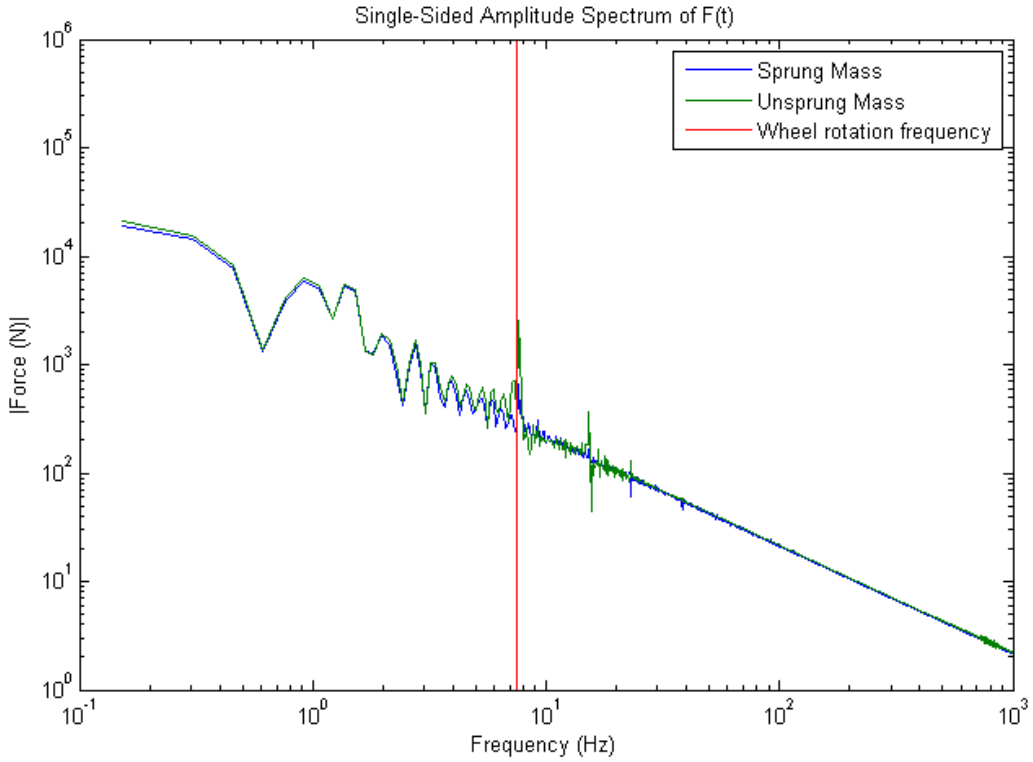

Figure 20 – Vertical force amplitude as a function of frequency.

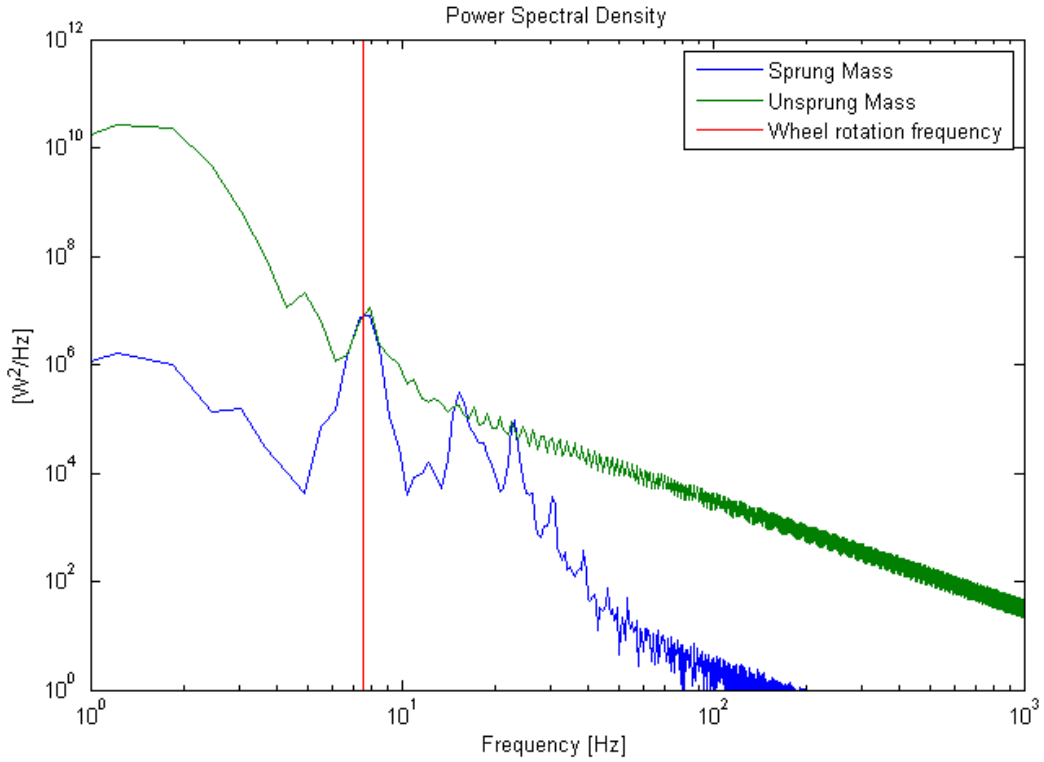

Figure 21 – Power spectral density graph.

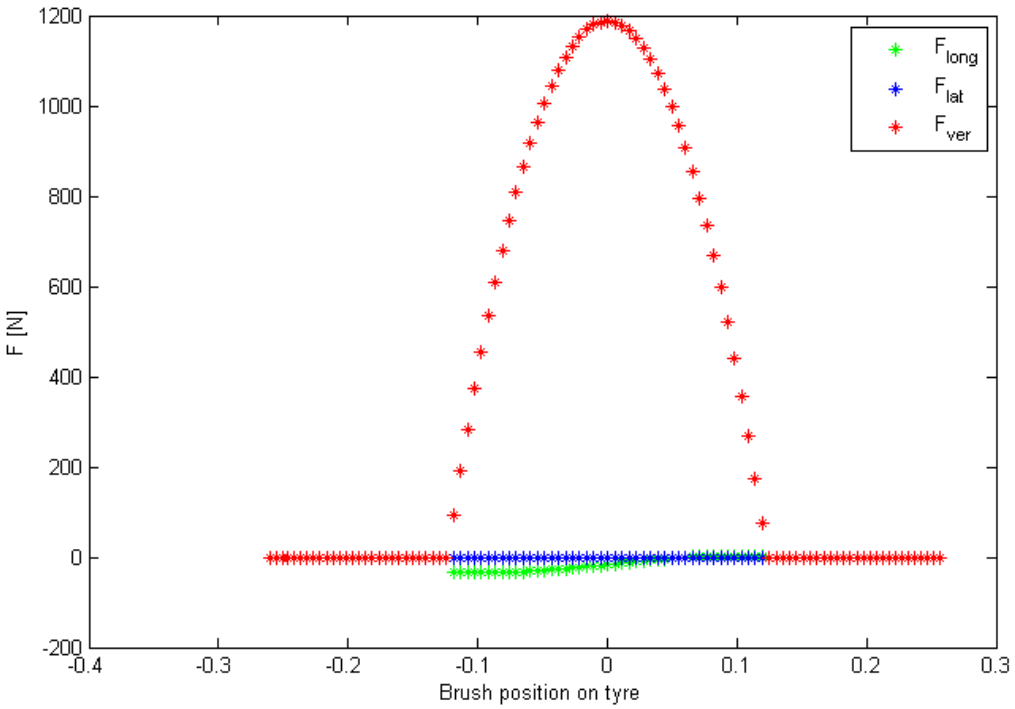

Figure 22 – Bristles forces as a function of their position on the tire.

7.3 Load case 3

Load case 3 shows a tire affected by radial run-out of the 1st harmonic, with a 0.005 m difference. The results are presented in Figures 23-26.

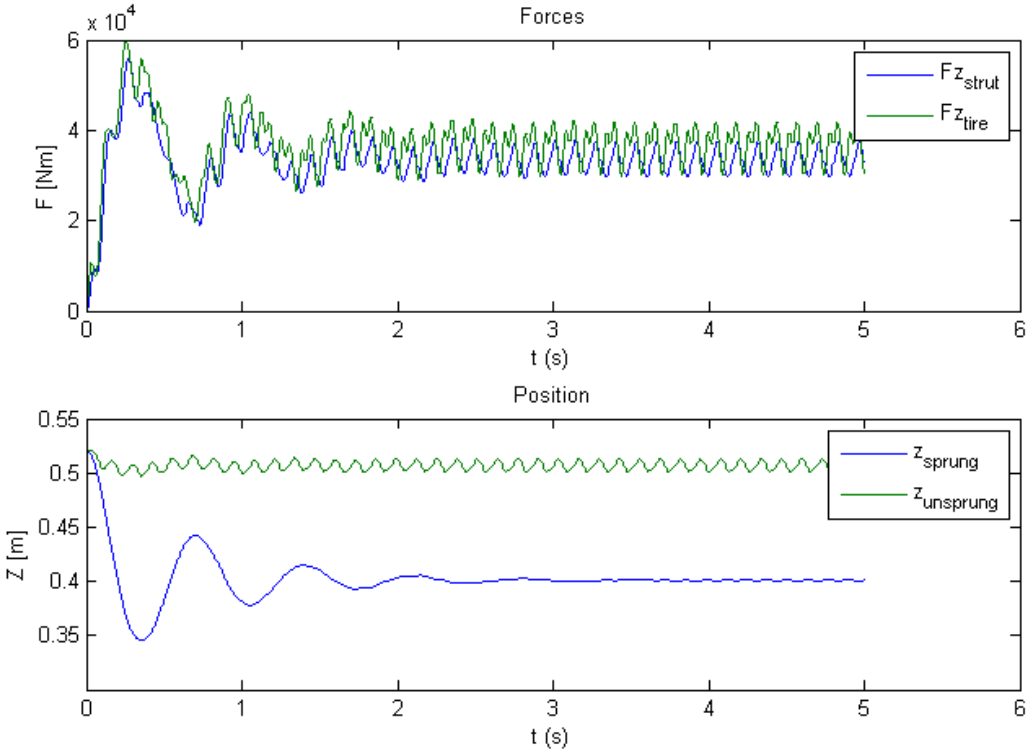

Figure 23 – Vertical forces and positions of sprung and unsprung masses, as a function of time.

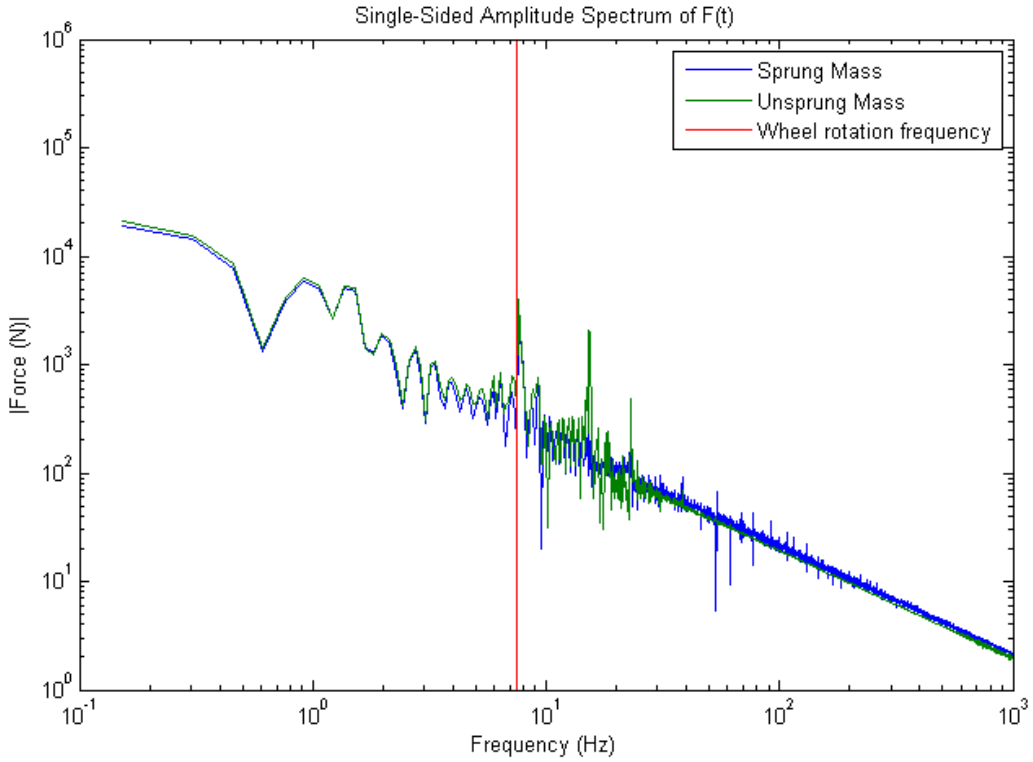

Figure 24 – Vertical force amplitude as a function of frequency.

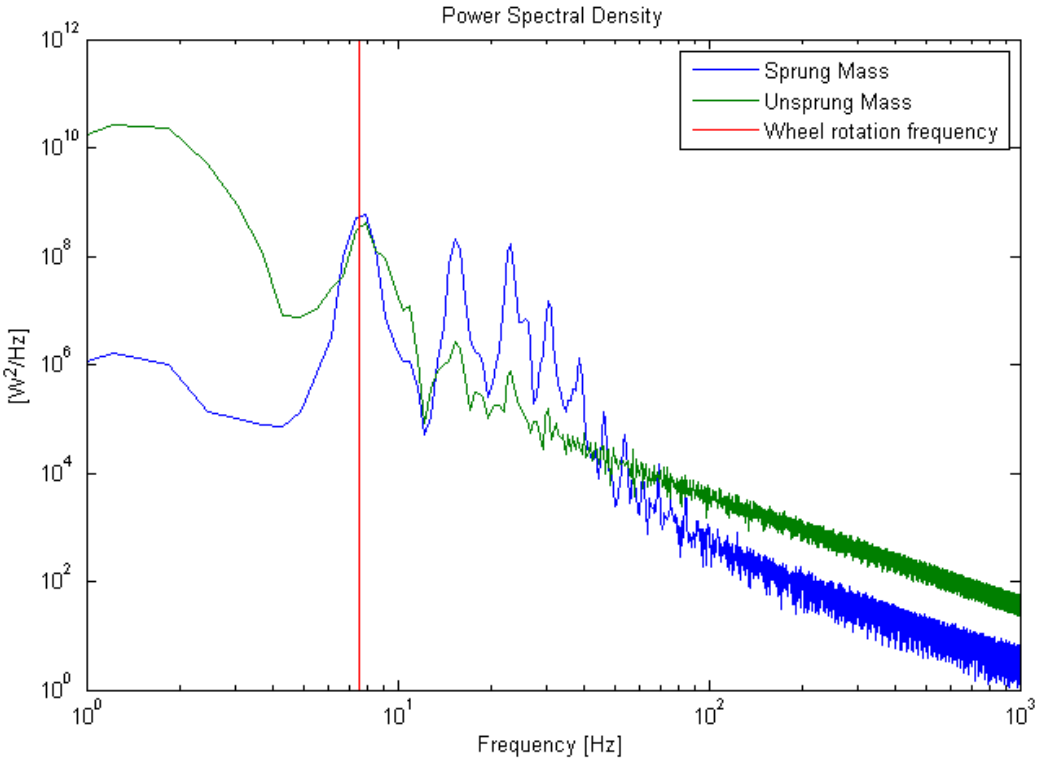

Figure 25 – Power spectral density graph.

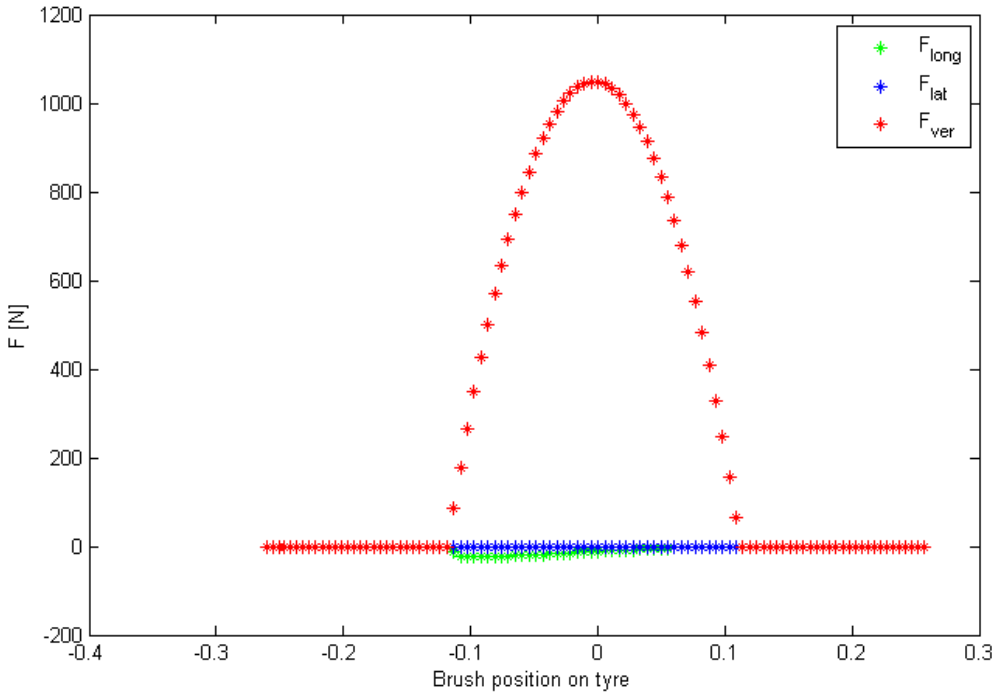

Figure 26 – Bristles forces as a function of their position on the tire.

7.4 Load case 4

Load case 4 presents a tire with a radial run-out of the 2nd harmonic. The difference in radius is 5 mm in two places opposite to each other, making the tire oval. See results in Figures 27-30.

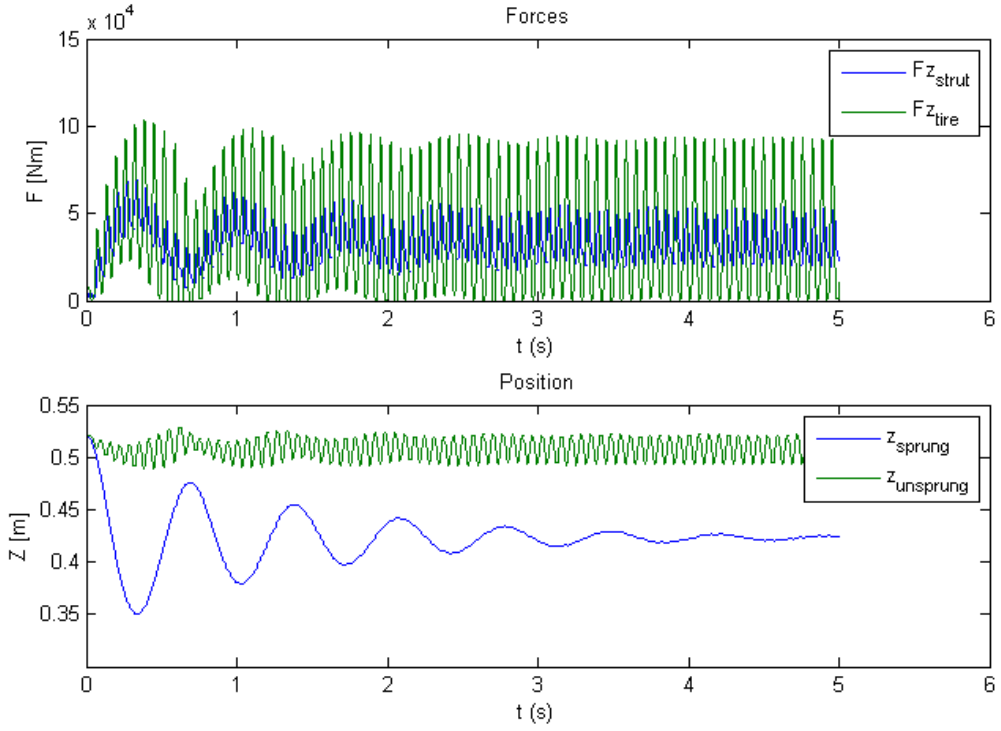

Figure 27 – Vertical forces and positions of sprung and unsprung masses, as a function of time.

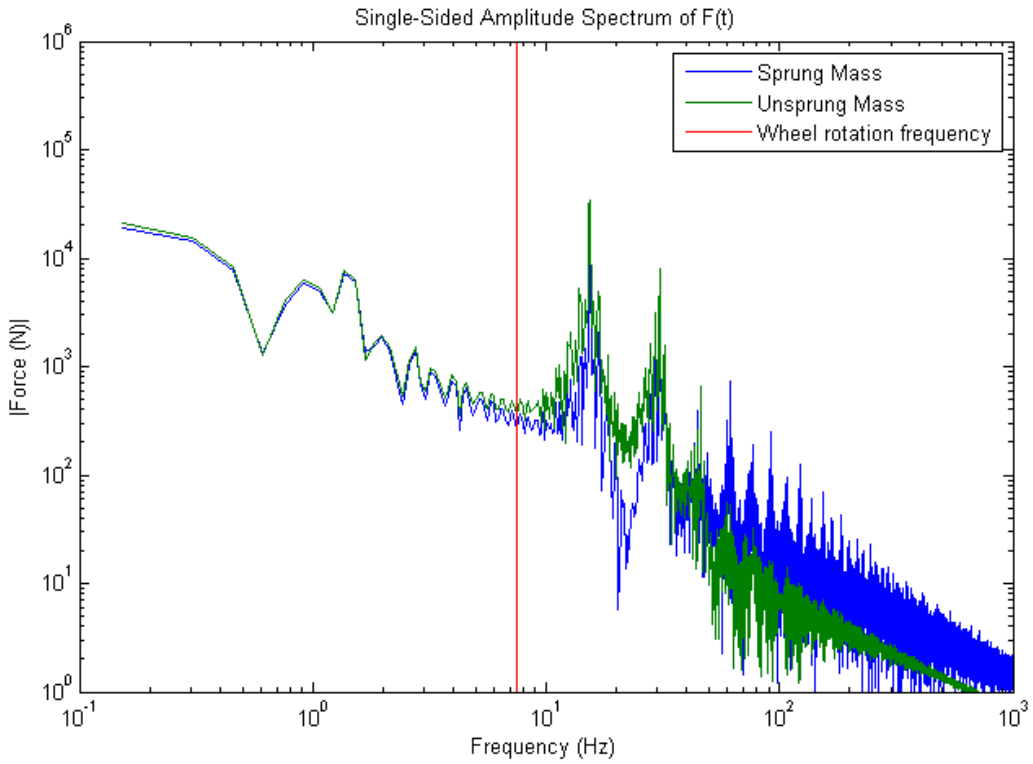

Figure 28 – Vertical force amplitude as a function of frequency.

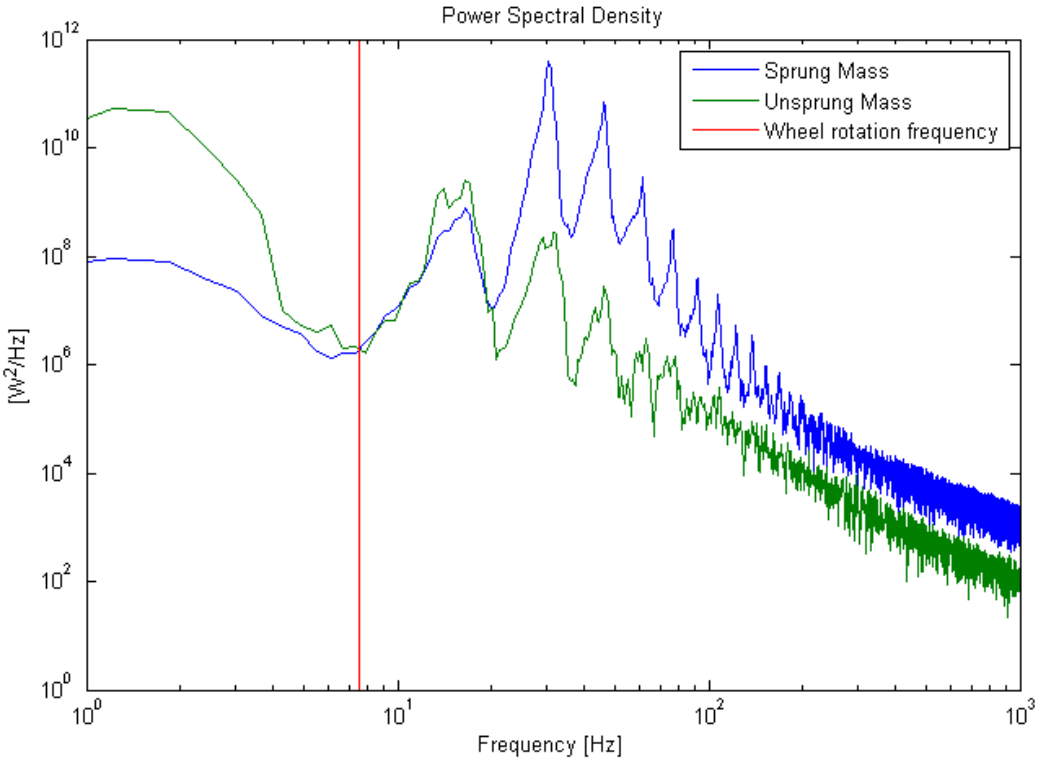

Figure 29 – Power spectral density graph.

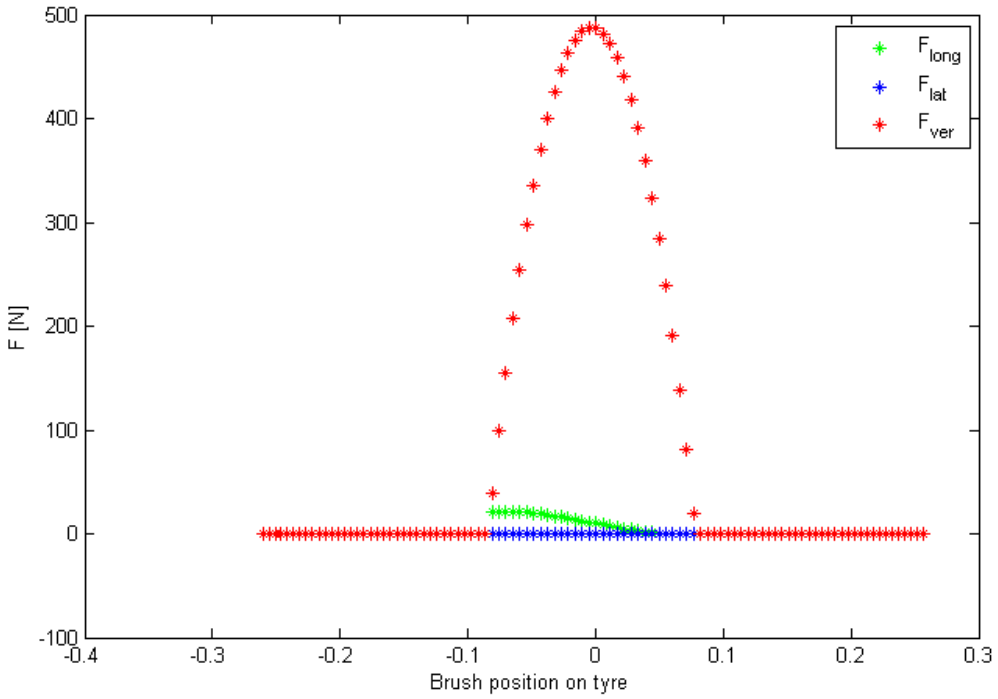

Figure 30 – Bristles forces as a function of their position on the tire.

7.5 Load case 5

Load case 5 presents a tire with a radial run-out of the 3rd harmonic. The difference in radius is 5 mm in three places along the circumference. Results are shown in Figures 31-34.

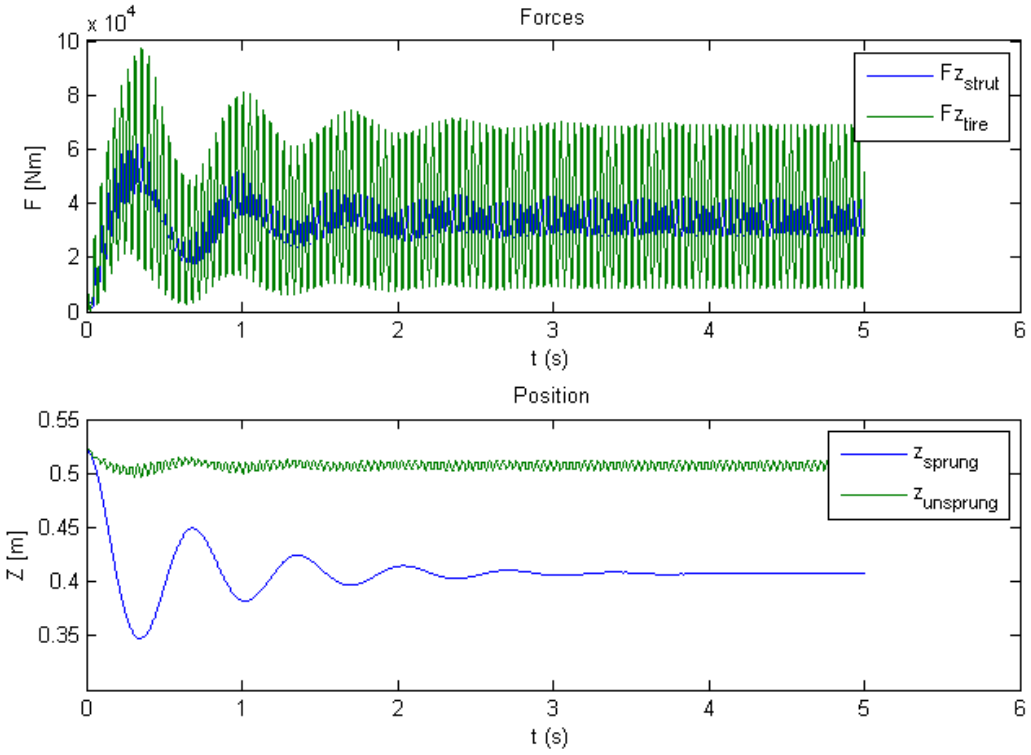

Figure 31 – Vertical forces and positions of sprung and unsprung masses, as a function of time.

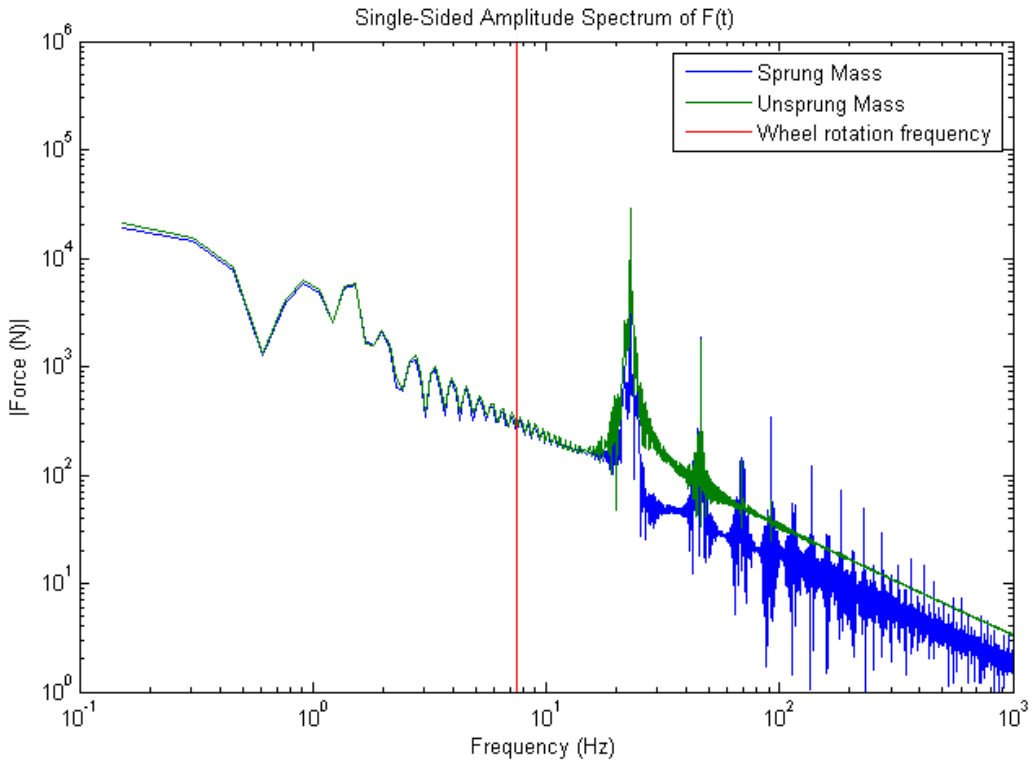

Figure 32 – Vertical force amplitude as a function of frequency.

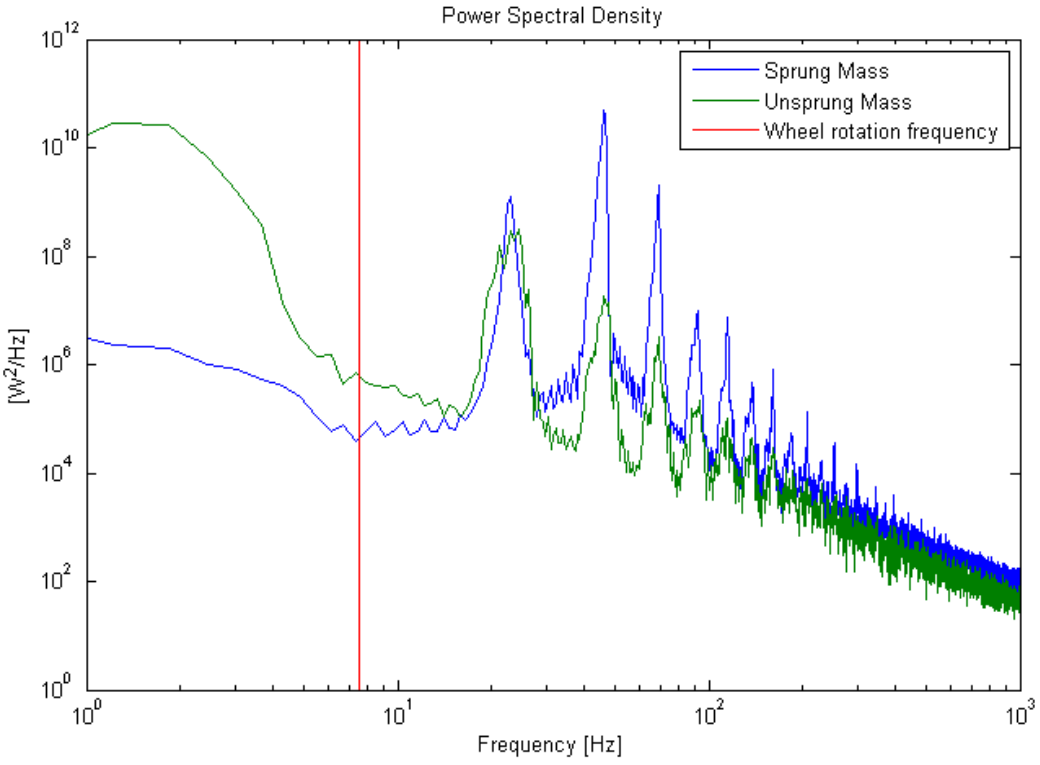

Figure 33 – Power spectral density graph.

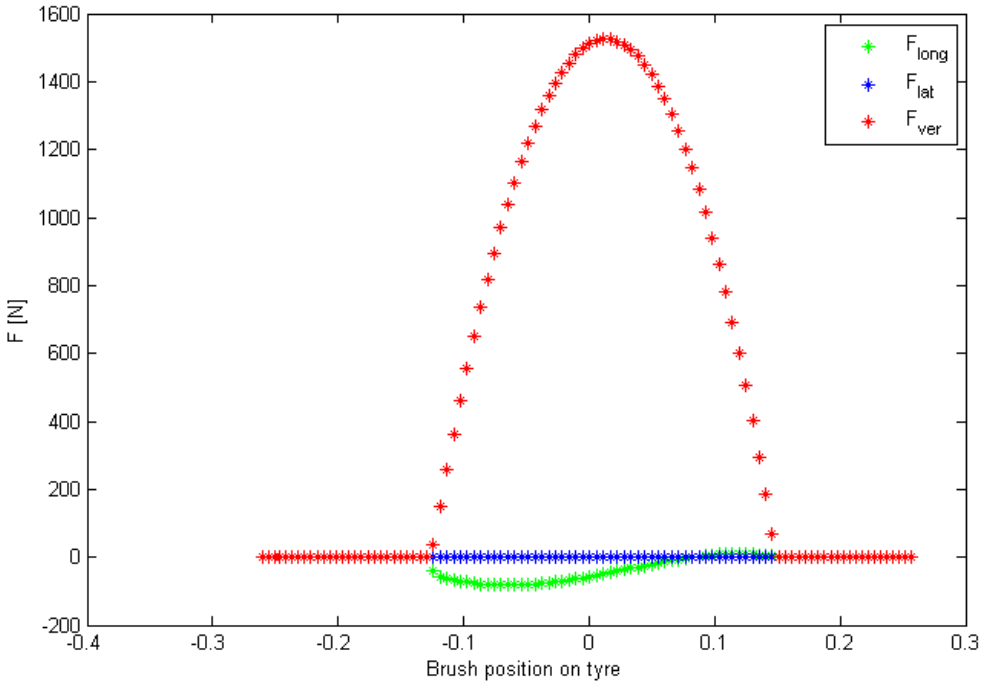

Figure 34 – Bristles forces as a function of their position on the tire.

7.6 Load case 6

Load case 6 presents a tire with a radial run-out of the 4th harmonic. The difference in radius is 5 mm in four places evenly spaced along the circumference, making the tire seem square. For results, see Figures 35-38.

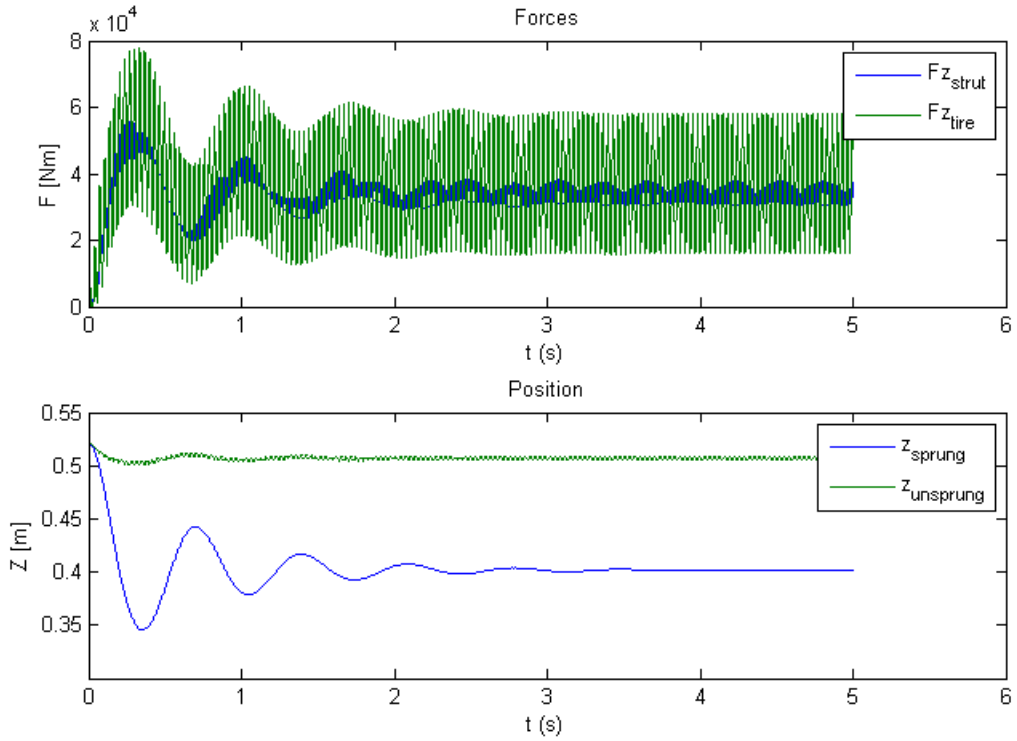

Figure 35 – Vertical forces and positions of sprung and unsprung masses, as a function of time.

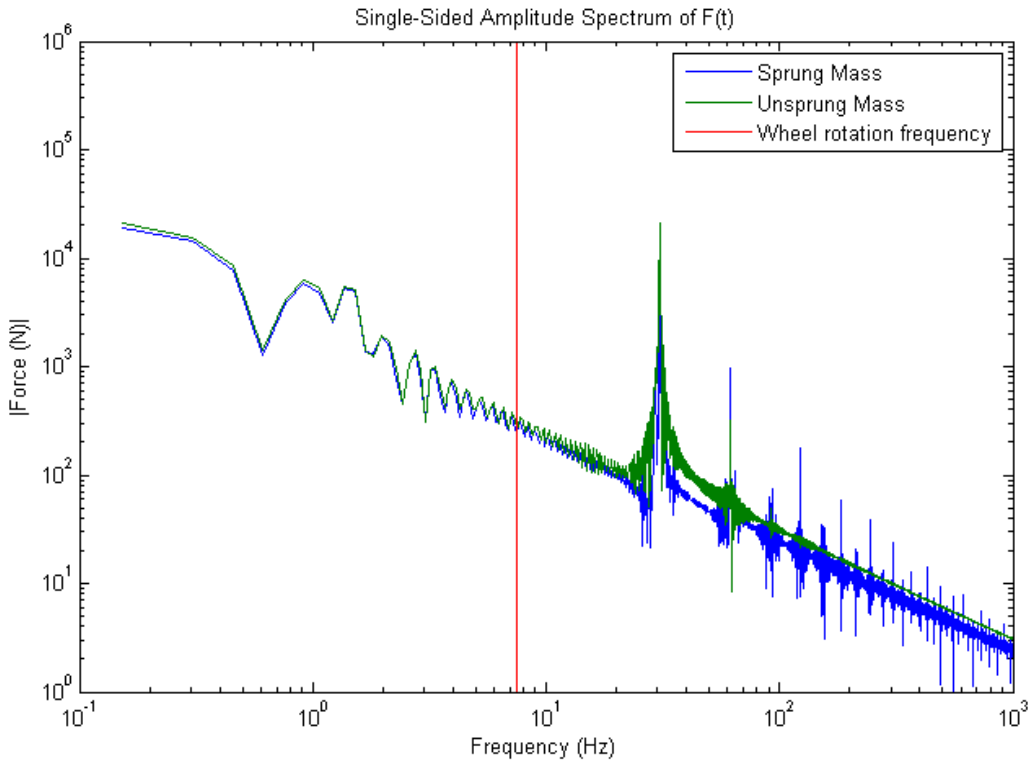

Figure 36 – Vertical force amplitude as a function of frequency.

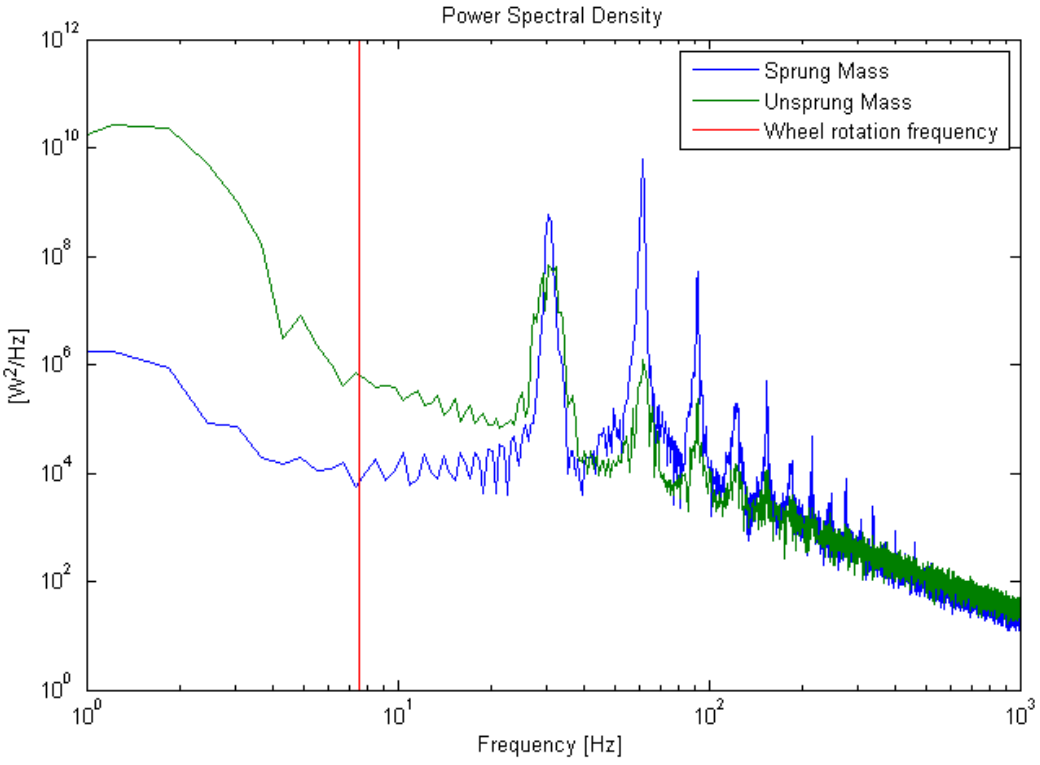

Figure 37 – Power spectral density graph.

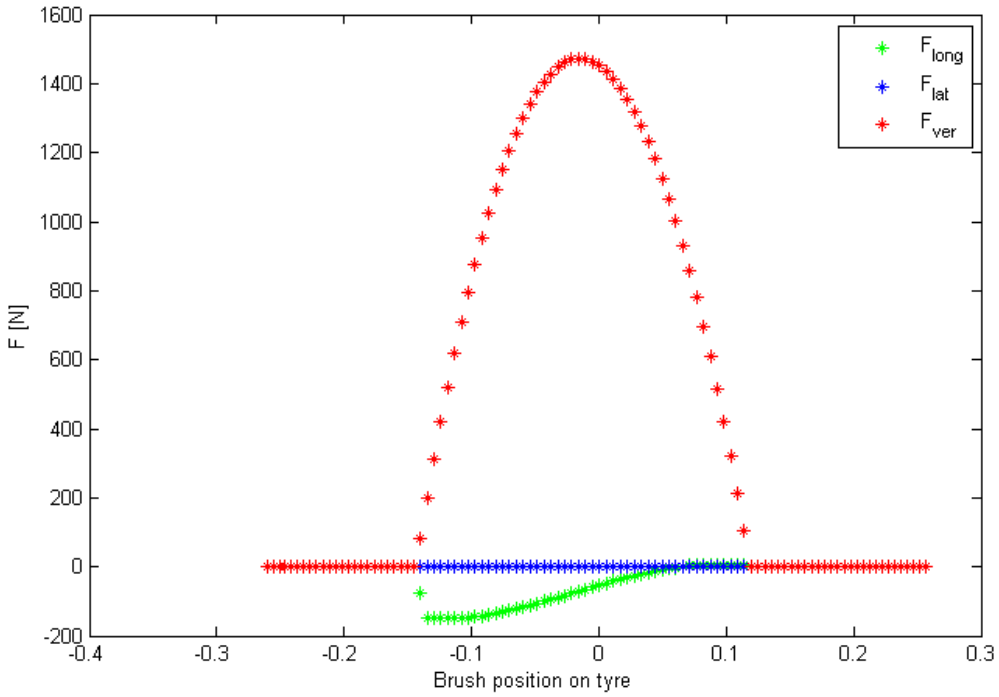

Figure 38 – Bristles forces as a function of their position on the tire.

7.7 Load case 7

The tire in this load case is affected by a mass imbalance of 2 kg on circumference, a 90 degrees phase shift, and a 1st harmonic radial run-out. Results are shown in Figures 39-42.

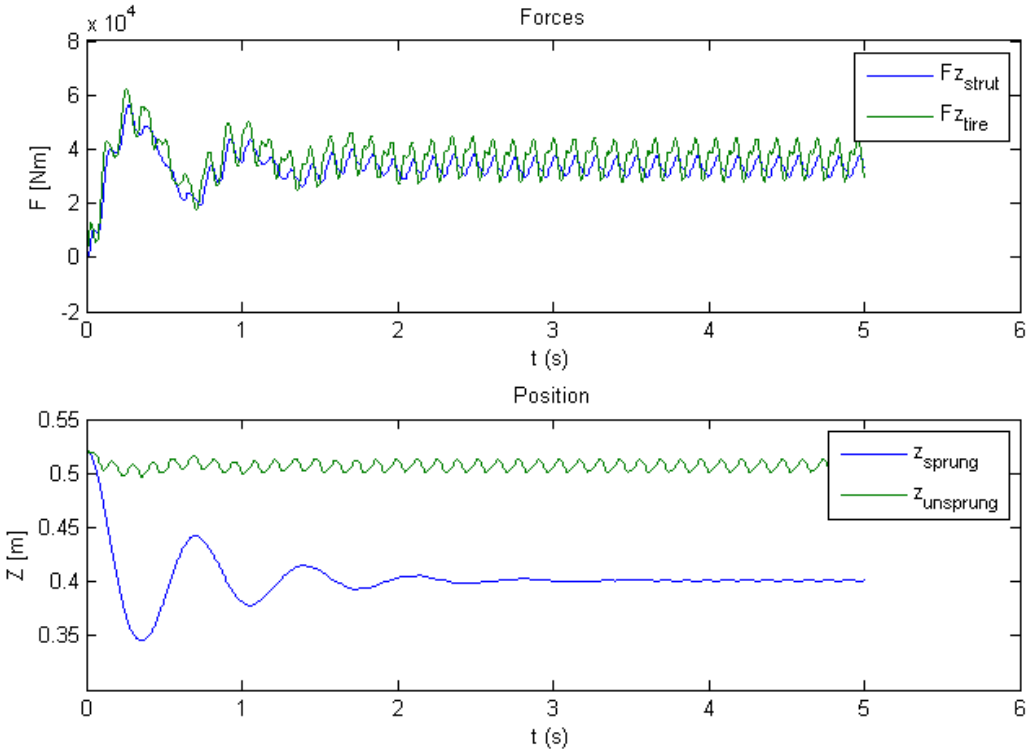

Figure 39 – Vertical forces and positions of sprung and unsprung masses, as a function of time.

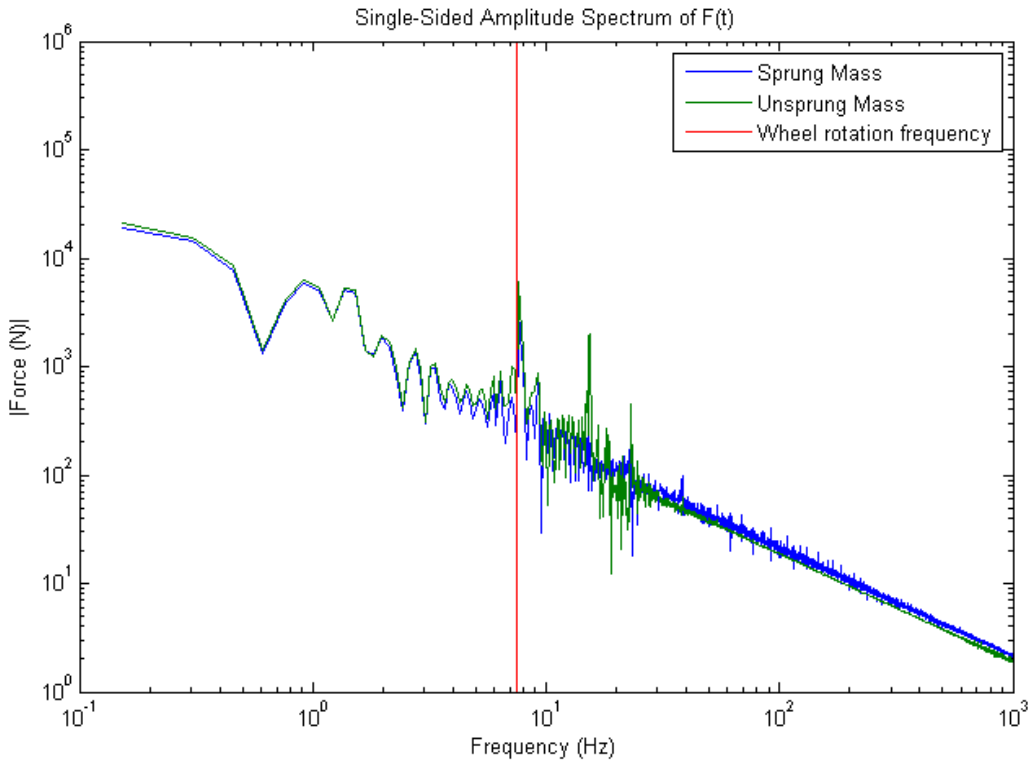

Figure 40 – Vertical force amplitude as a function of frequency.

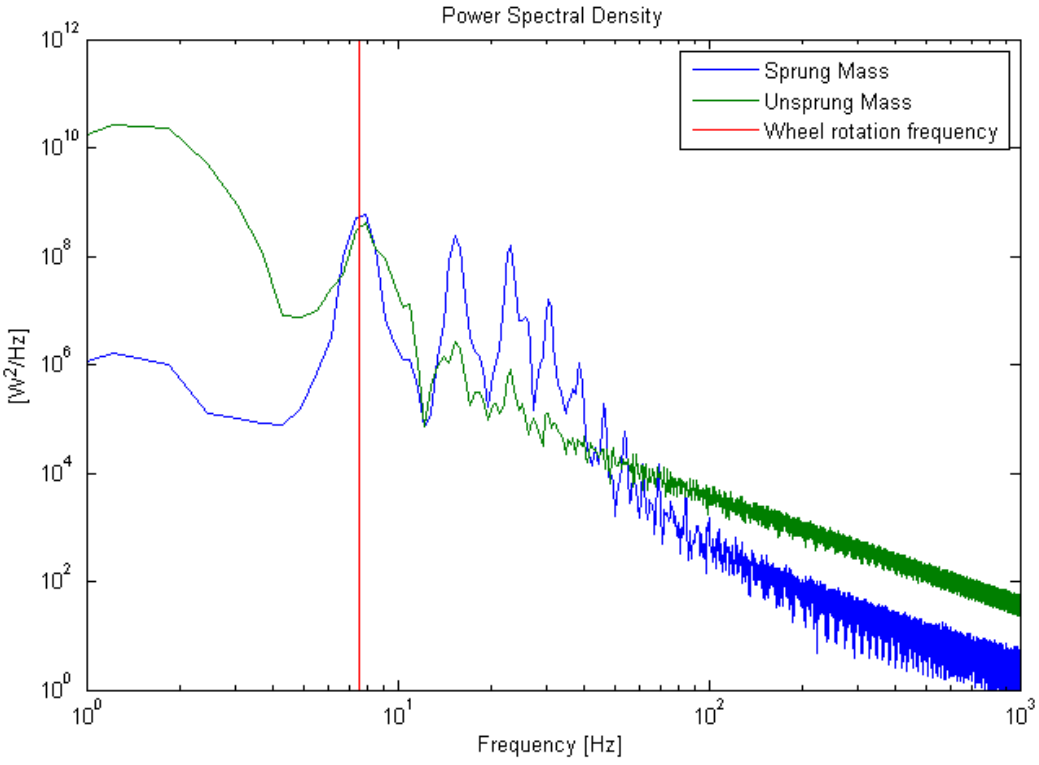

Figure 41 – Power spectral density graph.

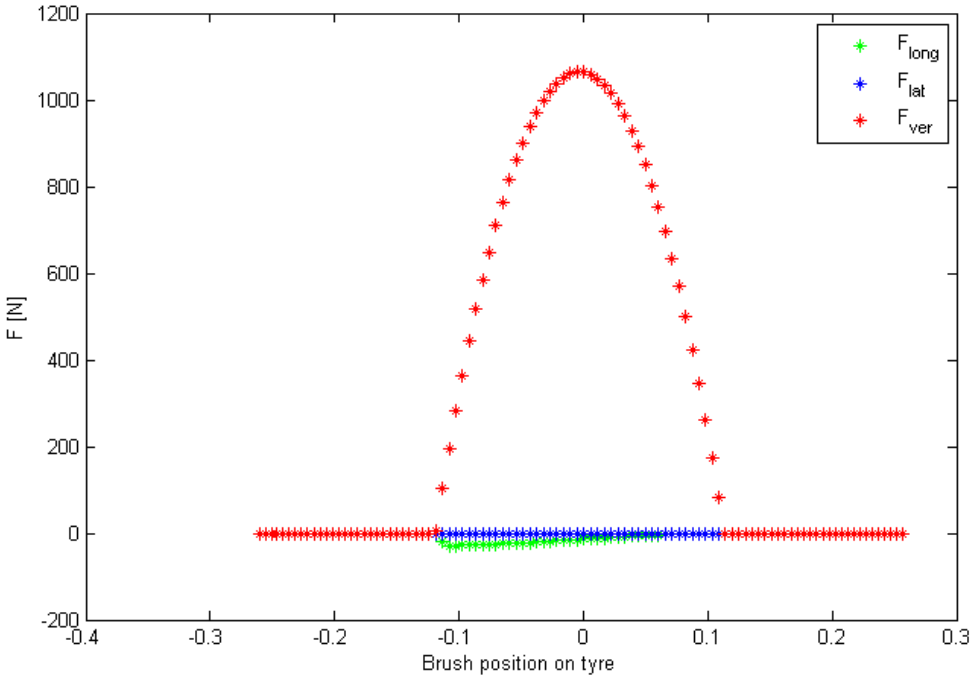

Figure 42 – Bristles forces as a function of their position on the tire.

7.8 Load case 8

This load case is made up of two different load cases, both affected by a mass imbalance; one of 8 kg and the other of 0.5 kg, both on the circumference. Results are shown in Figures 43-45.

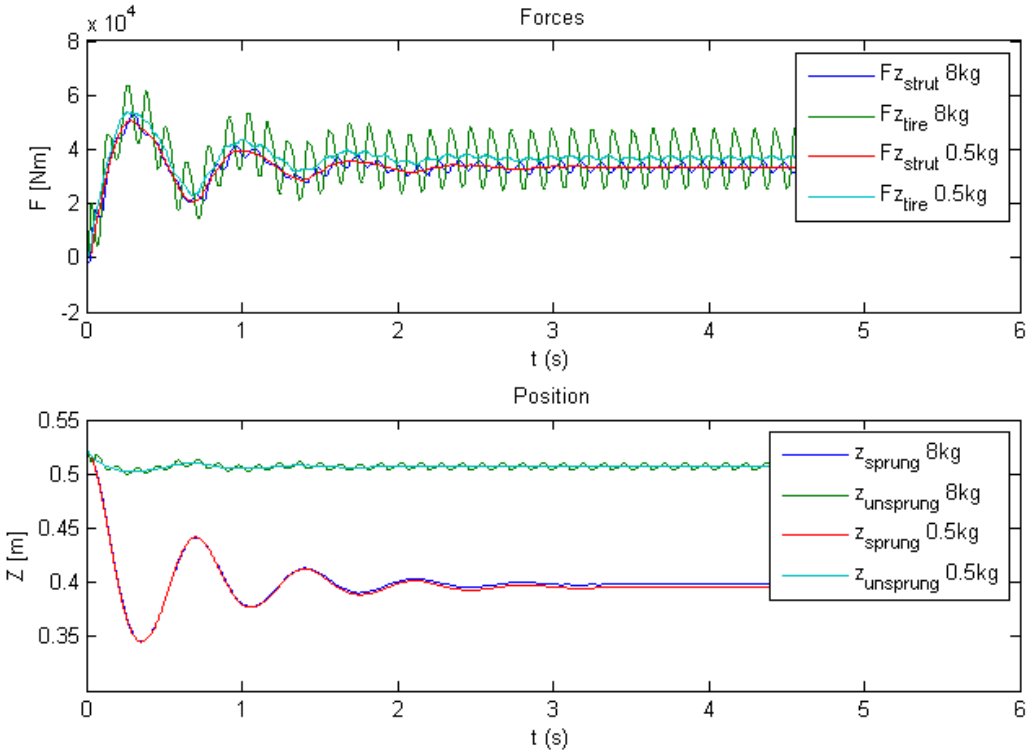

Figure 43 – Vertical forces and positions of sprung and unsprung masses, as a function of time.

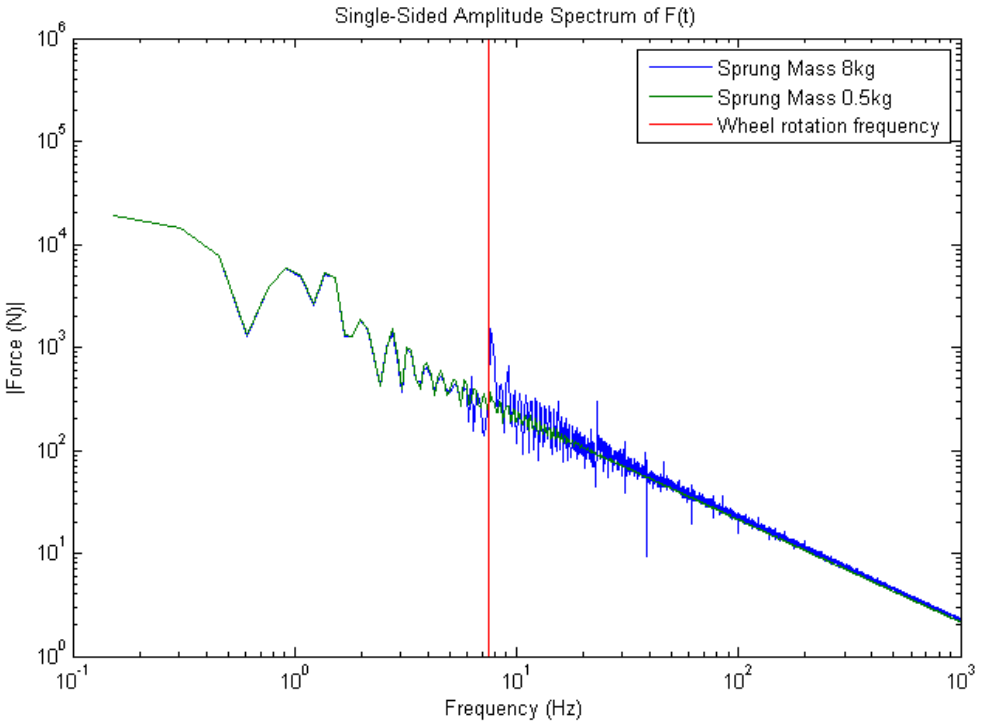

Figure 44 – Vertical force amplitude as a function of frequency.

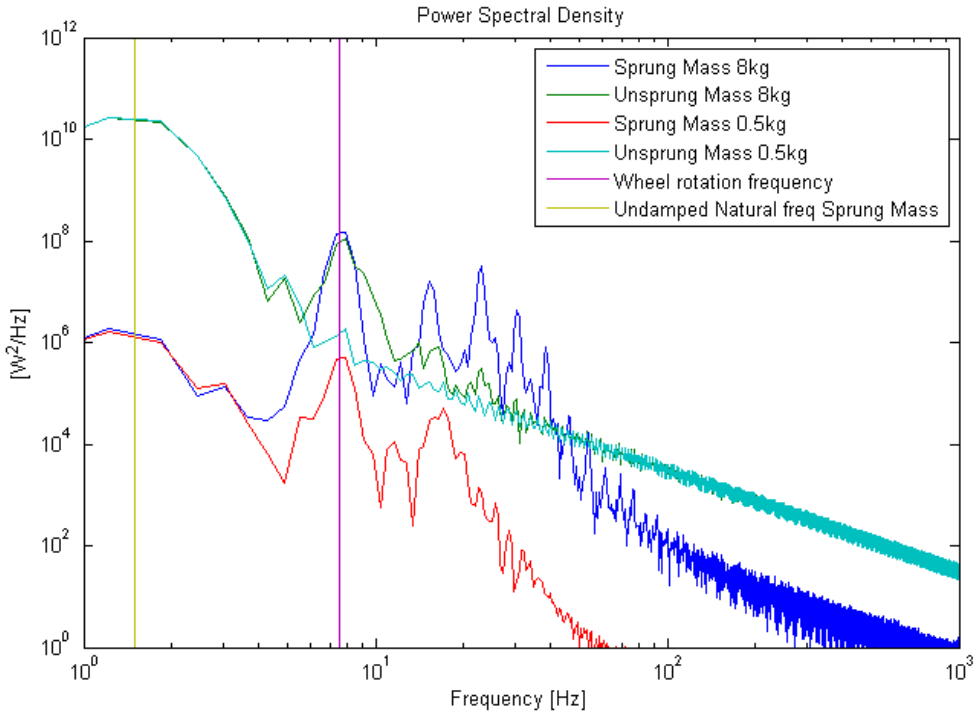

Figure 45 – Power spectral density graph.

8. Appendix B – MATLAB-script

```
%%%%% Main Script Wheel Induced Vibrations
%%%%% Hector Garcia && Emma Smith
%%%%% 2013-05-16

clear all
close all
clc
plotrate=0.0001; %How often visualisation

%Quarter car init
mass=3400;                          %Sprung mass
mt=350;                             %Unsprung mass
k=300000;                           %suspension spring stiffness
d=3000;                             %suspension damping coefficient this is not
the used value see function "damper"
g=9.82;                             %Gravity
my=1;
mu = 2;                             %mass of mass imbalance
radiu = 0.5;                        %Radius of mass imbalance
rotoffcenter = -pi/2*0;               %phasedifference of mass imbalance



wheel_radius=1.0435/2;
%% Init the brush model (create memory structure)
[A,B]=init_Bm(wheel_radius);

dt=0.005;       %time step for simulation
time=0;         %Starting time
tstop=3;       %stoptime
j=1;
l=0;


Wtlost(1)=0;


%init
az=[0];vz=[0];z=[wheel_radius];zt=[wheel_radius];vzt=[0];azt=[0];Vyc=-
3;pt=[0];ps=[0];
Fx=0;Fy=0;Fz=0;Mx=0;My=0;Mz=0;Mz_x=0;Mz_y=0;Fs=0;
x=0;
roll_angle=0;
jj=1;
step = 1;

aviobj = avifile('Monsters University AAAAAWWWWWWW
YEAH!!.avi','compression','none','fps',24,'quality',100);

while time<=tstop

Vxc=24.72;          %Long velocity of wheel centre
Vyc=0;           %lat velocity of wheel centre
yaw_rate=0;      %affect lateral speed along contact line
w=(Vxc*1.0172)/wheel_radius*1.0;  %Rollong speed in rad/s of wheel
```

```
%% Call brush model
[Fx(j+1),Fy(j+1),Fz(j+1),Mz(j+1),A,B,F]=brush(A,B,x(j),zt(j),Vxc,Vyc,vzt(j)
,w,yaw_rate,my,dt,roll_angle(j));

if jj>=plotrate;

brushvisu(A,B,Fx(j),Fy(j),Fz(j),zt(j),Vxc,Vyc,x(j),F,roll_angle(j),time,z(j
),wheel_radius);
    fig=figure(70);
    Fr=getframe(fig);
    aviobj=addframe(aviobj,Fr);
    jj=0;
    step = step+1;
else
    jj=jj+1;
end




%% quarter car model
Fs(j+1)=(k*(zt(j)-z(j))+damper(vzt(j)-vz(j)));   %strut force from spring
and damper
%% motion of suspended mass (car body)
az(j+1)=Fs(j+1)/mass-g;  %Strut force acting on sprung mass
vz(j+1)=vz(j)+az(j+1)*dt;
z(j+1)=z(j)+vz(j+1)*dt;
%% motion of unsuspended mass (wheel)
Fb(j+1) = mu*radiu*(w^2)*sin(roll_angle(j)+rotoffcenter);
azt(j+1)=(Fz(j+1)-Fs(j+1)+Fb(j+1))/mt-g; %Tyre pushing up strut pushing
down
vzt(j+1)=vzt(j)+azt(j+1)*dt;
zt(j+1)=zt(j)+vzt(j+1)*dt;

x(j+1)=x(j)+Vxc*dt;
roll_angle(j+1)=roll_angle(j)+w*dt;

time=time+dt;



%% Power of suspended mass
pt(j+1) = Fs(j+1)*(z(j+1)-z(j))/dt;                          %Unsprung mass
ps(j+1) = (Fz(j+1)-Fs(j+1)+Fb(j+1))*(zt(j+1)-zt(j))/dt;      %Sprung mass

j=j+1;
t(j)=time;

end

aviobj = close(aviobj);
clear aviobj

% %%% Following part is used only when two mass imbalance imperfections is
% %%% simulated
% %% Init the brush model (create memory structure)
% mu2 = 0.5;                          %mass of massunbalance
```

```
% radiu = 0.5;                     %Radius of mass unbalance
% rotoffcenter = -pi/2*0;          %phasedifference of massunbalance
%
% [A,B]=init_Bm(wheel_radius);
%
% dt=0.0001;       %time step for simulation
% time=0;
% tstop=5;       %stoptime
% j=1;
% l=0;
%
%
% Wtlost(1)=0;
%
%
% %init
%
az2=[0];vz2=[0];z2=[wheel_radius];zt2=[wheel_radius];vzt2=[0];azt2=[0];Vyc2
=-3;pt2=[0];ps2=[0];
% Fx2=0;Fy2=0;Fz2=0;Mx2=0;My2=0;Mz2=0;Mz_x2=0;Mz_y2=0;Fs2=0;
% x=0;
% roll_angle=0;
% jj=1;
% while time<=tstop
%
% Vxc=24.72;          %Long velocity of wheel centre
% Vyc=0;           %lat velocity of wheel centre
% yaw_rate=0;      %affect lateral speed along contact line
% w=(Vxc*1.0172)/wheel_radius*1.0;  %Rollong speed in rad/s of wheel
%
% %% Call brush model
%
[Fx2(j+1),Fy2(j+1),Fz2(j+1),Mz2(j+1),A,B,F]=brush2(A,B,x(j),zt2(j),Vxc,Vyc,
vzt2(j),w,yaw_rate,my,dt,roll_angle(j));
%
% if jj>=plotrate;
% %
brushvisu(A,B,Fx(j),Fy(j),Fz(j),zt(j),Vxc,Vyc,x(j),F,roll_angle(j),time,z(j
))
%     jj=0;
% else
%     jj=jj+1;
% end
%
%
%
%
% %% quarter car model
% Fs2(j+1)=(k*(zt2(j)-z2(j))+damper(vzt2(j)-vz2(j)));   %strut force from
spring and damper
% %% motion of suspended mass (car body)
% az2(j+1)=Fs2(j+1)/mass-g;  %Strut force acting on sprung mass
% vz2(j+1)=vz2(j)+az2(j+1)*dt;
% z2(j+1)=z2(j)+vz2(j+1)*dt;
% %% motion of unsuspended mass (wheel)
% Fb2(j+1) = mu2*radiu*(w^2)*sin(roll_angle(j)+rotoffcenter);
% azt2(j+1)=(Fz2(j+1)-Fs2(j+1)+Fb2(j+1))/mt-g; %Tyre pushing up strut
pushing down
% vzt2(j+1)=vzt2(j)+azt2(j+1)*dt;
% zt2(j+1)=zt2(j)+vzt2(j+1)*dt;
%
```

```
% x(j+1)=x(j)+Vxc*dt;
% roll_angle(j+1)=roll_angle(j)+w*dt;
%
% time=time+dt;
%
%
%
% %% Power of suspended mass
% pt2(j+1) = Fs2(j+1)*(z2(j+1)-z2(j))/dt;
% ps2(j+1) = (Fz2(j+1)-Fs2(j+1)+Fb2(j+1))*(zt2(j+1)-zt2(j))/dt;
%
% j=j+1;
% t(j)=time;
%
%
% end

%% Undamped Natural frequencies
Tire_circumference = 2*pi*wheel_radius;
rps = Vxc/Tire_circumference            %Wheel rotation frequency
nfreq_body = sqrt(k/mass)/(2*pi)        %Undamped natural frequency of
sprung mass
nfreq_tire = sqrt((k+8000000)/mt)/(2*pi)    %Undamped natural ferquency of
unsprung mass

%% Tire and Strut forces during the whole simulation together with vertical
%% position of the tire and chassi
figure(1)
subplot(2,1,1)
plot(t,Fs,t,Fz)%,t,Fs2,t,Fz2)%,t,Mz);
legend('Fz_s_t_r_u_t','Fz_t_i_r_e')%,'Fz_s_t_r_u_t 0.5kg','Fz_t_i_r_e
0.5kg')%,'Mz')
title('Forces')
ylabel('F [Nm]')
xlabel('t (s)')
subplot(2,1,2)
plot(t,z,t,zt)%,t,z2,t,zt2);
legend('z_s_p_r_u_n_g','z_u_n_s_p_r_u_n_g')%'z_s_p_r_u_n_g
8kg','z_u_n_s_p_r_u_n_g 8kg','z_s_p_r_u_n_g 0.5kg','z_u_n_s_p_r_u_n_g
0.5kg')
title('Position')
xlabel('t (s)')
ylabel('Z [m]')

%% Momentanius Forces in the bristles
x_pos=sin(A(1,:))*wheel_radius;
fx=F(1,:);
fy=F(2,:);
fz=F(3,:);
figure(2)
plot(x_pos,fx,'g*',x_pos,fy,'b*',x_pos,fz,'r*')
legend('F_l_o_n_g','F_l_a_t','F_v_e_r')
xlabel('Brush position on tyre')
ylabel('F [N]')


%% Fourier Analysis
figure(3)
% subplot(2,1,1)
Fsamp = 1/plotrate; %Sampling frequency
```

```
L = length(az);
NFFT = 2^nextpow2(L);
YFt = fft(Fz,NFFT)/L;      %Fast Fourier Transform
YFs = fft(Fs,NFFT)/L;       %Fast Fourier Transform
f = Fsamp/2*linspace(0,1,NFFT/2+1);
loglog(f,2*abs(YFs(1:NFFT/2+1)),f,2*abs(YFt(1:NFFT/2+1)),[rps rps],[1
10^6])
title('Single-Sided Amplitude Spectrum of F(t)')
legend('Sprung Mass 8kg','Sprung Mass 0.5kg','Wheel rotation frequency')
xlabel('Frequency (Hz)')
ylabel('|Force (N)|')
axis([0.1 1000 1 10^6])


%% PSD Calculation
figure(4)
% subplot(2,1,2)
% wh = hamming(L/40);
% noverlap = NFFT/2;
% [Pz2,wz2] = pwelch(ps2);
% wz2 = wz2*10000/(2*pi);
[Pz1,wz] = pwelch(ps);
wz = wz*10000/(2*pi);
% [Pzt2,wt2] = pwelch(pt2);
% wt2 = wt2*10000/(2*pi);
[Pzt1,wt] = pwelch(pt);
wt = wt*10000/(2*pi);
loglog(wz,Pz1,wt,Pzt1,[rps rps],[1 10^12])%,wz2,Pz2,wt2,Pzt2,[rps rps],[1
10^12],[nfreq_body nfreq_body],[1 10^12])%,[nfreq_tire nfreq_tire],[1
10^12])
% loglog([rps rps],[1 10^12], 'k')              %Rolling freq
% loglog([nfreq_body nfreq_body],[1 10^12], 'k')%Body undamped natural
frequency
% loglog([nfreq_tire nfreq_tire],[1 10^12], 'k')%Tire undamped natural
frequency
legend('Sprung Mass 8kg','Unsprung Mass 8kg','Sprung Mass 0.5kg','Unsprung
Mass 0.5kg','Wheel rotation frequency','Undamped Natural freq
Body')%,'Undamped Natural freq tire')
title('Power Spectral Density')
xlabel('Frequency [Hz]')
ylabel('[W^2/Hz]')
axis([1 1000 1 10^12])
% text(3,10^11,'Rolling frequency');
```

```
%%% Brush Model
%%% Johannes Edrén

function
[Fx,Fy,Fz,Mz,Bristle_deflec,B,F]=brush(Bristle_deflec,B,x,zt,Vxc,Vyc,vzt,w,
yaw_rate,my,dt,roll_angle)
%Tyre_Data=[Rr,cpx,cpy,cpz,dpz,load_sensetivity,segment_angle,f_pz0];
Rw=B(1);cpx=B(2);cpy=B(3);cpz=B(4);dpx=B(5);dpz=B(6);load_sensetivity=B(7);
segment_angle=B(8);
f_pz0=B(9);D_amp=B(10);D_periode=B(11);
n=length(Bristle_deflec);
phi_step=w*dt;

    for i =1:n;
    xpos=Rw*sin(Bristle_deflec(1,i));
    Bristle_deflec(1,i)=Bristle_deflec(1,i)-phi_step; %update rolling of
bristles along the segment

    %move/update rolling of the bristles in and out of the segment of
    %bristles (move the last bristle to the front and vice versa)
    if Bristle_deflec(1,i)<-segment_angle/2
        Bristle_deflec(1,i)=Bristle_deflec(1,i)+segment_angle;
        Bristle_deflec(5,i)=1;
    end
    if Bristle_deflec(1,i)>segment_angle/2
        Bristle_deflec(1,i)=Bristle_deflec(1,i)-segment_angle;
        Bristle_deflec(5,i)=1;
    end

    %vertical displacement of the bristles
    %% z deflection
    %Bristle_deflec(4,i)=zt-Rw*cos(Bristle_deflec(1,i))-road(xpos+x);
    Bristle_deflec(4,i)=zt-
cos(Bristle_deflec(1,i))*(Rw+D_amp*sin((Bristle_deflec(1,i)+roll_angle)/D_p
eriode*2*pi))-road(xpos+x);
    %dzdt(i)=Rw*sin(Bristle_deflec(1,i))*w;
    dzdt(i)=Rw*sin(Bristle_deflec(1,i))*w;  % OBS not corret atm. Only
sping forces are correct

    if Bristle_deflec(4,i)>=0       %if the brush is not in contact with
the road
        Bristle_deflec(2,i)=0;      %no deflection in x
        Bristle_deflec(3,i)=0;      %no deflection in y
        Bristle_deflec(4,i)=0;      %no deflection in z
        in_contact(i)=0;            %if a brush is in contact r not

      d_x(i)=0;
      d_y(i)=0;
    else% deflection of each bristle
        %d_x(i)=w*dt*Rw*cos(Bristle_deflec(1,i))-Vxc*dt;      %Longitudinal
incremantal displacement of each bristle

d_x(i)=w*dt*(Rw+D_amp*sin((Bristle_deflec(1,i)+roll_angle)/D_periode*2*pi))
*cos(Bristle_deflec(1,i))-Vxc*dt;
        old_deflecx(i)=Bristle_deflec(2,i);
        Bristle_deflec(2,i)=old_deflecx(i)+d_x(i);
    %Lateral incremental displacement of each bristle
        d_y(i)=-Vyc*dt + -
(Rw+D_amp*sin((Bristle_deflec(1,i)+roll_angle)/D_periode*2*pi))*sin(Bristle
_deflec(1,i))*yaw_rate*dt;
```

```
        old_deflecy(i)=Bristle_deflec(3,i);
        Bristle_deflec(3,i)=old_deflecy(i)+d_y(i);
        in_contact(i)=1;
    end
    %vertical force on each bristle
    fz(i)=-Bristle_deflec(4,i)*cpz+dzdt(i)*dpz*in_contact(i);
    %fz(i)=-Bristle_deflec(4,i)*cpz;
    if fz(i)<=0;
        fz(i)=0;
    end
    %total force of bristle in x and y
    fx(i)=Bristle_deflec(2,i)*cpx;
    fy(i)=Bristle_deflec(3,i)*cpy;
    total(i)=sqrt(fx(i)^2+fy(i)^2);
    %if deflection times stiffness larger than force
    fxprim(i)=fx(i);
    fyprim(i)=fy(i);


Worg(i)=(fx(i)*Bristle_deflec(2,i)+fy(i)*Bristle_deflec(3,i))*in_contact(i)
;

    if abs(total(i))>my*fz(i);
        pdf=0.05*10^(-2)*0.1; %power dissipation when slipping
        Bristle_deflec(5,i)=Bristle_deflec(5,i)-
sqrt(d_x(i)^2+d_y(i)^2)*my*fz(i)/dt*pdf;

        fyprim(i)=fy(i)*my*fz(i)/(total(i)+eps)*Bristle_deflec(5,i);
        fxprim(i)=fx(i)*my*fz(i)/(total(i)+eps)*Bristle_deflec(5,i);


%% limit the force to friction
        Bristle_deflec(2,i)=fxprim(i)/cpx;
        Bristle_deflec(3,i)=fyprim(i)/cpy;
        fx(i)=Bristle_deflec(2,i)*cpx;
        fy(i)=Bristle_deflec(3,i)*cpy;
    %else
    %    Bristle_deflec(5,i,id)=1;

    end

eta(i)=sqrt(fx(i)^2+fy(i)^2)/fz(i);

    end

dfz=(sum(fz)-f_pz0)/f_pz0;
fx=fx*(1-load_sensetivity*dfz);
fy=fy*(1-load_sensetivity*dfz);


Mz=sum(fy.*sin(Bristle_deflec(1,:))*Rw);


Fx= sum(fx);
Fy= sum(fy);
Fz= sum(fz); %tyre vertical force from ground
F(1,:)=fx;
```

```
F(2,:)=fy;
F(3,:)=fz;



%%% Visualisation of Brush Model

%%% Johannes Edrén with minor modifications by Hector Garcia
%%% 2013-05-16

function
brushvisu(A,B,Fx,Fy,Fz,zt,Vxc,Vyc,x,F,roll_angle,t,bz,wheel_radius)
Bristle_deflec=A;
Rw=B(1);
cpx=B(6);
cpy=B(7);
cpz=B(8);D_amp=B(10);D_periode=B(11);
phi=linspace(-pi,pi,200);

innerRx=sin((phi)).*(Rw+D_amp*sin((phi+roll_angle)/D_periode*2*pi));
innerRz=-cos((phi)).*(Rw+D_amp*sin((phi+roll_angle)/D_periode*2*pi));

inX=(Rw-D_amp)*sin((phi-roll_angle));
inZ=(Rw-D_amp)*cos((phi-roll_angle));
medX=(Rw)*sin((phi-roll_angle));
medZ=(Rw)*cos((phi-roll_angle));
outX=(Rw+D_amp)*sin((phi-roll_angle));
outZ=(Rw+D_amp)*cos((phi-roll_angle));


sf=0.0001;%Scale factor for force visualisation

X=linspace(-0.5,0.5,100);
for i=1:length(X)
    Z(i)=road(X(i)+x);
    Y(i)=0;
end

scrsz = get(0,'ScreenSize');

figure(70)
hold off
clf
% figure('NextPlot','replacechildren','OuterPosition',[1 scrsz(4)/2
scrsz(3)/2 scrsz(4)/2]) %'ColorSpec',[1 1 1],
        subplot(1,2,1)
        plot(innerRx,innerRz+zt,'-k');%tyre shape
        hold on
        plot(inX,inZ+zt,'-r');%inner diameter
        plot(outX,outZ+zt,'-r');%outerm diameter
        %plot(medX,medZ+zt,'-b');%median diameter
        for i=1:length(A)
            %z0=zt-Rw*cos(Bristle_deflec(1,i));
            z0=zt-
cos(Bristle_deflec(1,i))*(Rw+D_amp*sin((Bristle_deflec(1,i)+roll_angle)/D_p
eriode*2*pi));
            z1=z0-Bristle_deflec(4,i);
            %z2=z1+F(3,i)*sf;
            %x0=Rw*sin(Bristle_deflec(1,i));
```

```
x0=sin(Bristle_deflec(1,i))*(Rw+D_amp*sin((Bristle_deflec(1,i)+roll_angle)/
D_periode*2*pi));
            x1=x0+Bristle_deflec(2,i);
            %x2=x1+F(1,i)*sf;
            %y0=0;
            %y1=y0+Bristle_deflec(3,i);
            %y2=y1+F(2,i)*sf;

            %red color for slipping brisltle and blue color for sticking
            if Bristle_deflec(5,i)<0.995 && Bristle_deflec(4,i)~=0;
                plot([x0 x1],[z0 z1],'-r');
            else
                plot([x0 x1],[z0 z1],'-b');
            end
             plot([-0.5 0.5],[bz+1 bz+1],'r','LineWidth',3)
        end
            plot([0 Rw*sin(roll_angle)],[zt zt+Rw*cos(roll_angle)],'k');
%Rotating Line

            plot([0 Fx*sf],[0 0],'r');
            plot([0 0],[0 Fz*sf],'r');
            plot([0 0],[0 Vxc/20],'b','LineWidth',2);
            plot(X,Z)
            text(0.05,0.275,num2str(t)); %plots time.
            axis equal
            grid on
            %axis([-0.5 0.5 -0.1 0.7]);
            axis([-1 1 -0.1 2]);


            subplot(1,2,2)
            x_pos=sin(A(1,:))*wheel_radius;
            fx=F(1,:);
            fy=F(2,:);
            fz=F(3,:);
            %figure(2)
            plot(x_pos,fx,'g*',x_pos,fy,'b*',x_pos,fz,'r*')
            legend('F_l_o_n_g','F_l_a_t','F_v_e_r')
            xlabel('Brush position on tyre')
            ylabel('F [N]')
            axis([-0.3 0.3 -500 2000]);




drawnow
```

```
%%% Damper Function
%%% Hector Garcia

function F=damper(vz)

dcomp=2000;          %Damping constant in Compression
dexp=20000;          %Damping constant in Expansion
if vz <= 0
    F=vz*dcomp;
else
    F=vz*dexp;
end
end
```

```
%%% Initialization of Brushmodel with Tire Imperfections
%%% Johannes Edrén

function [Bristle_deflec,Tyre_Data]=init_Bm(Wheel_radius)

f_pz0=9.82*350;%nominal tyre load;

%parameters
n=100;                              %Number or bristles of the segment
[Parameter]
segment_angle=pi/3;                 %segment angle [Parameter]

dpx=0;
dpz=500/n*0;                      %vertical bristle damping per unit length
[parameter]

load_sensetivity=0.15;
angle_between_segments=segment_angle/(n);
Rr=Wheel_radius;

cpy=1000000/(n/4);                     %lateral bristle stiffness per unit
length  [parameter]
cpx=1000000/(n/4);                     %longitudinal bristle stiffness per
unit length [parameter]
cpz=2000000/(n/4);                     %vertical bristle stiffness per unit
length

%% un roundness of the tyre
D_amp = 0.005*0; %[m]
D_periode = 2*pi; %[rad] ; =2*pi for off centre tyre, should always be
<=2*pi!!

Tyre_Data=[Rr,cpx,cpy,cpz,dpx,dpz,load_sensetivity,segment_angle,f_pz0,D_am
p,D_periode];

%% init for brush tyre model
%phi=linspace(-segment_angle/2,segment_angle/2,n+1);         % only check
brushes in contact from -segment_angle/2 to +segment_angle/2 degrees
phi=[-segment_angle/2:angle_between_segments:segment_angle/2-
angle_between_segments];
```

```
Bristle_deflec=zeros(5,n);                                  %History of
deflections for the bristles [angle,dx,dy,dz] This structure needs to be
know from previous time step
Bristle_deflec(1,:)=phi;            %Starting values of phi of all the
bristles.
Bristle_deflec(5,:)=ones(1,n);
```

```
%%% Road Imperfections
%%% Johannes Edrén

function z=road(x)
%Road disturbance z as function of long position x
%% Flat
z=0;
Amp=0.05;                   %Amplitude of disturbance
%% sine disturbance
%  z=Amp*sin(x*10);         %Use for a sine disturbance
%% step disturbance at 10
% z=0;
% if x>5
%     z=Amp;
% end


end
```

```
%%% Brush Model for second calculation
%%% Hector Garcia
%%% 2013-05-16


function
[Fx2,Fy2,Fz2,Mz2,Bristle_deflec,B,F]=brush2(Bristle_deflec,B,x,zt2,Vxc,Vyc,
vzt2,w,yaw_rate,my,dt,roll_angle)
%Tyre_Data=[Rr,cpx,cpy,cpz,dpz,load_sensetivity,segment_angle,f_pz0];
Rw=B(1);cpx=B(2);cpy=B(3);cpz=B(4);dpx=B(5);dpz=B(6);load_sensetivity=B(7);
segment_angle=B(8);
f_pz0=B(9);D_amp=B(10);D_periode=B(11);
n=length(Bristle_deflec);
phi_step=w*dt;

    for i =1:n;
    xpos=Rw*sin(Bristle_deflec(1,i));
    Bristle_deflec(1,i)=Bristle_deflec(1,i)-phi_step; %update rolling of
bristles along the segment

    %move/update rolling of the bristles in and out of the segment of
    %bristles (move the last bristle to the front and vice versa)
    if Bristle_deflec(1,i)<-segment_angle/2
        Bristle_deflec(1,i)=Bristle_deflec(1,i)+segment_angle;
        Bristle_deflec(5,i)=1;
    end
    if Bristle_deflec(1,i)>segment_angle/2
```

```
        Bristle_deflec(1,i)=Bristle_deflec(1,i)-segment_angle;
        Bristle_deflec(5,i)=1;
    end

    %vertical displacement of the bristles
    %% z deflection
    %Bristle_deflec(4,i)=zt-Rw*cos(Bristle_deflec(1,i))-road(xpos+x);
    Bristle_deflec(4,i)=zt2-
cos(Bristle_deflec(1,i))*(Rw+D_amp*sin((Bristle_deflec(1,i)+roll_angle)/D_p
eriode*2*pi))-road(xpos+x);
    %dzdt(i)=Rw*sin(Bristle_deflec(1,i))*w;
    dzdt(i)=Rw*sin(Bristle_deflec(1,i))*w;  % OBS not corret atm. Only
sping forces are correct

    if Bristle_deflec(4,i)>=0       %if the brush is not in contact with
the road
        Bristle_deflec(2,i)=0;      %no deflection in x
        Bristle_deflec(3,i)=0;      %no deflection in y
        Bristle_deflec(4,i)=0;      %no deflection in z
        in_contact(i)=0;            %if a brush is in contact r not

      d_x(i)=0;
      d_y(i)=0;
    else% deflection of each bristle
        %d_x(i)=w*dt*Rw*cos(Bristle_deflec(1,i))-Vxc*dt;      %Longitudinal
incremantal displacement of each bristle

d_x(i)=w*dt*(Rw+D_amp*sin((Bristle_deflec(1,i)+roll_angle)/D_periode*2*pi))
*cos(Bristle_deflec(1,i))-Vxc*dt;
        old_deflecx(i)=Bristle_deflec(2,i);
        Bristle_deflec(2,i)=old_deflecx(i)+d_x(i);
    %Lateral incremental displacement of each bristle
        d_y(i)=-Vyc*dt + -
(Rw+D_amp*sin((Bristle_deflec(1,i)+roll_angle)/D_periode*2*pi))*sin(Bristle
_deflec(1,i))*yaw_rate*dt;

        old_deflecy(i)=Bristle_deflec(3,i);
        Bristle_deflec(3,i)=old_deflecy(i)+d_y(i);
        in_contact(i)=1;
    end
    %vertical force on each bristle
    fz(i)=-Bristle_deflec(4,i)*cpz+dzdt(i)*dpz*in_contact(i);
    %fz(i)=-Bristle_deflec(4,i)*cpz;
    if fz(i)<=0;
        fz(i)=0;
    end
    %total force of bristle in x and y
    fx(i)=Bristle_deflec(2,i)*cpx;
    fy(i)=Bristle_deflec(3,i)*cpy;
    total(i)=sqrt(fx(i)^2+fy(i)^2);
    %if deflection times stiffness larger than force
    fxprim(i)=fx(i);
    fyprim(i)=fy(i);


Worg(i)=(fx(i)*Bristle_deflec(2,i)+fy(i)*Bristle_deflec(3,i))*in_contact(i)
;

    if abs(total(i))>my*fz(i);
        pdf=0.05*10^(-2)*0.1; %power dissipation when slipping
```

```
        Bristle_deflec(5,i)=Bristle_deflec(5,i)-
sqrt(d_x(i)^2+d_y(i)^2)*my*fz(i)/dt*pdf;

        fyprim(i)=fy(i)*my*fz(i)/(total(i)+eps)*Bristle_deflec(5,i);
        fxprim(i)=fx(i)*my*fz(i)/(total(i)+eps)*Bristle_deflec(5,i);


%% limit the force to friction
        Bristle_deflec(2,i)=fxprim(i)/cpx;
        Bristle_deflec(3,i)=fyprim(i)/cpy;
        fx(i)=Bristle_deflec(2,i)*cpx;
        fy(i)=Bristle_deflec(3,i)*cpy;
    %else
    %    Bristle_deflec(5,i,id)=1;

    end

eta(i)=sqrt(fx(i)^2+fy(i)^2)/fz(i);

    end

dfz=(sum(fz)-f_pz0)/f_pz0;
fx=fx*(1-load_sensetivity*dfz);
fy=fy*(1-load_sensetivity*dfz);


Mz2=sum(fy.*sin(Bristle_deflec(1,:))*Rw);


Fx2= sum(fx);
Fy2= sum(fy);
Fz2= sum(fz); %tyre vertical force from ground
F(1,:)=fx;
F(2,:)=fy;
F(3,:)=fz;
```